TECHNICAL MEMORANDUM

222

Sensitivity of ECMWF model wintertime climate to model formulation

Č. Branković and F. Molteni

Research Department

November 1995

European Centre for Medium-Range Weather Forecasts
Europäisches Zentrum für mittelfristige Wettervorhersage
Centre européen pour les prévisions météorologiques à moyen

Abstract

The impact of various model formulations on model climate during boreal winter is studied from ensembles of seasonal integrations for four different versions of the ECMWF NWP model. The model versions, cycles 36, 46, 48 and 12r1, differ primarily in the representation of physical parametrization. In addition, higher vertical resolution was used for the 12r1 integrations.

In the more recent cycles (48 and 12r1) a strong systematic overestimation of zonal flow over the northeastern Pacific has been dramatically reduced, contributing to a more realistic representation of the Pacific block. This improved representation of blocking, particularly in cycle 12r1, is linked to a more efficient diabatic response of the model to the warm SSTs in the western Pacific. In contrast, over the Atlantic/European region a slight deterioration of blocking frequency in cycle 12r1 is associated with the strengthening of the Atlantic jet. The improvement in the southern hemisphere circulation, already evident in cycle 46, is not seen in the northern hemisphere, so it is argued that the impact of radiation changes introduced between cycle 36 and cycle 46 (inclusive) is influenced by seasonal cycle. A strong cooling of the southern (summer) polar stratosphere has been steadily reduced and in cycle 12r1 is about a half of that seen in cycle 36. A reduction of errors in zonally averaged zonal wind and eddy kinetic energy is also clearly seen. In the tropics, the Hadley circulation has become more intense with the later cycles. This is associated with an intensification of convective rainfall within relatively narrow tropical convergence zones.

The representation of interannual variations between strong positive and negative ENSO-index winters was most successful in cycle 12r1; however, in the both later cycles, 48 and 12r1, the simulation of interannual variations has become more sensitive to flow-dependent errors. The frequency of observed hemispheric clusters is found to be best reproduced by cycle 12r1.

1. Introduction

A knowledge of the climate of a global numerical weather prediction (NWP) model or a general circulation model (GCM) is nowadays essential to assess the model's performance and its deficiencies. The model climate is normally derived from a number of relatively long, extended-range model integrations. The departure of the model climate from some observed mean state of the atmosphere, usually referred to as the climate drift (or equivalently as the systematic error of the model predictions), largely depends on the nature of the deficiencies in the model formulation. Systematic differences with respect to the real atmospheric state may also be influenced by "external" factors, such as the way the lower boundary forcing is formulated. However, we consider here only the drift induced by deficiencies intrinsic to the model. In short or medium range forecasts, model systematic errors may not always manifest themselves strongly enough to be detectable with high statistical significance; therefore the study of model climate drift on longer time scales may help to better define and understand the systematic effects of errors in model formulation, and eventually lead to their correction. On the other hand, relatively strong systematic errors in the short or medium-range period may be due to a relatively fast "adjustment" of the model atmosphere, and a simple extrapolation of these errors in time may lead to a wrong estimate of the equilibrium model climate. Fig.2 in Palmer *et al.* (1990) demonstrates this "two-way" relationship between medium-range systematic errors and "long-term" climate drift from a relatively large set of European Centre for Medium-Range Weather Forecasts (ECMWF) monthly forecasts.

In the continual effort to improve the accuracy of NWP, it is necessary to modify frequently the formulation of a numerical model in order to introduce more efficient numerical schemes and more accurate or detailed parametrizations of physical processes. Changes to the model formulation necessarily influence systematic errors and ultimately model climate.

In this paper we assess various aspects of the impact of some modifications to the formulation of the ECMWF NWP model on the model climate during northern winter. Four versions of the ECMWF operational model were studied. These model versions are denoted as model cycles 36, 46, 48 and 12r1 with cycle 12r1 being the latest. For each cycle of the model, the model climate was derived from seasonal integrations in a consistent fashion. By comparing the climates derived from various model versions, we also document the evolutionary improvements of the ECMWF model (see also discussion on climates of the NCAR Community Climate Model by Hurrell 1995).

In the following section a brief summary of meteorological changes introduced with model cycles 36, 46, 48 and 12r1 is given. In section 3 the organisation of experiments used in estimating the model climate is described. Section 4 deals with upper-air wintertime circulation, mainly in terms of errors (drift) and differences among the four model cycles. The impact of model changes on precipitation is discussed in section 5. The blocking frequency and circulation regime statistics are

given in section 6. In section 7 some aspects of the simulation of interannual variations are shown. Section 8 concludes the paper with a summary and discussion of our results.

2. Summary of changes to model formulation

Detailed descriptions of various numerical, physical and technical changes to the ECMWF model formulation are found in relevant ECMWF Research Department documentation. Only a brief summary of the model changes introduced with model cycles 36, 46, 48 and 12r1 is given below. Other changes to both physical and dynamical ECMWF model formulations were also introduced over the period since cycle 36 came into operations; the principal changes are listed in Table 1. Many of them were mainly of technical nature, and some, as for example the semi-Lagrangian dynamics and related modifications, are not relevant for this study as all runs are at T63 resolution and use an Eulerian time scheme (see the next section on organization of experiments).

Cycle 36 of the model (hereafter referred as CY36) was introduced in operations on 5 June 1990 and included several changes (Miller *et al.* 1992)[1]. The parametrization of surface fluxes at low wind speed over the sea was modified so that the latent heat flux over the warm pools increased dramatically. The convective cloud formulation was modified in order to account for radiative effects of non-precipitating shallow cumuli. The third modification was the introduction of an implicit formulation of gravity-wave drag parametrization. This model cycle was used for much of experimentation on the seasonal time scale. A detailed description of the CY36 climatology is given in Ferranti *et al.* (1994a) and extended range predictability using 3-member and 9-member ensembles respectively was discussed by Branković *et al.* (1994) and Branković and Palmer (1996).

Cycle 46 (CY46) was introduced in operations on 1 February 1993. The cloud and radiation parametrization had been modified to include shortwave optical properties for ice and mixed phase clouds, and in addition, the clear-sky absorption was revised (Morcrette 1993)[2]. Also, the horizontal diffusion was modified, but this is relevant only for the operational, T213, resolution of the model. The assessment of the model climatology for CY46 is important because of the introduction of an experimental Ensemble Prediction System (EPS) in the ECMWF operations in the same winter, 1992/93 (see Molteni *et al.* 1994).

Cycle 48 (CY48) was introduced in operations on 4 August 1993. The CY48 changes (Viterbo and Beljaars 1995) comprise the following[3]: (a) introduction of entrainment at the top of the planetary

[1] ECMWF Research Department Memos R2314/2618 and R2314/2617.

[2] ECMWF Research Department Memos R60.6.1/4/PA, R60.6.1/5/PA and R60.6.1/AS/302.

[3] ECMWF Research Department Memo R60.6.1/145/PA.

boundary layer (PBL), (b) increased entrainment in shallow clouds, (c) modified roughness length and air-sea transfer coefficients and (d) enhancements to the parametrization of the soil processes with four layers with prognostic variables for soil moisture and temperature, plus a skin layer temperature. Due to extensive modifications to the physical parametrization, one of the largest for several years, it was extremely important to assess the impact of CY48 changes on the model climatology.

Although cycle 12r1 was introduced in operations on 23 August 1994, it represented *per se* only some minor technical modifications to the previous cycle (11r7) which had been in operations since 2 March 1994. The adiabatic part of the model code had been completely rewritten in collaboration with Météo-France, and formed part of what is known as the Integrated Forecasting System (IFS). In the physical parametrization the following changes were made (also known as model cycle 50 in the pre-IFS convention)[4]. For the closure of the shallow convection scheme, the sensible heat flux is taken into account in addition to the latent heat flux. The second change was a correction of the latent heat release due to freezing of condensate in the convective updrafts together with a simple mixed-phase partitioning depending on temperature. In addition, the distinction between water and ice clouds in the radiation scheme was changed to be consistent with the distinction in the convection scheme.

In addition to the modifications in the model physics, our experiments with cycle 12r1 also included 31 levels in the vertical (see next section). It is important to emphasize that such an increased vertical resolution in the model certainly contributed to the changes in the model climate. However, based on the experience with further ECMWF experimentation, we assume that the impact of model physics modifications introduced with cycle 12r1 is dominant over that due to increased vertical resolution. Cases when this assumption is not appropriate will be explicitly discussed.

3. Experiment design

The experiments reported here with CY36, CY46 and CY48 were run at T63L19 model resolution. For cycle 12r1 there were 31 levels in the vertical, i.e. the model used was T63L31. (It has to be noted that 31 levels were introduced in the ECMWF operational model with model cycle 39, see Table 1.) The length of simulations was approximately 120 days, depending on initial date. The experimentation covers five winter seasons (DJF), from 1986/87 to 1990/91. For each winter three integrations initiated on the same calendar dates, 1, 2 and 3 November, were carried out. All experiments were run with Eulerian dynamics and on a full model grid.

[4] ECMWF Research Department Memo R60.6.1/21/PA

In the runs with CY36, CY46 and CY48, the observed sea surface temperature (SST) was updated every 5 days throughout the integration. In 12r1 on the other hand, the SST boundary forcing was updated in the model daily by interpolating from monthly average SSTs. It is assumed that this relatively small inconsistency in the SST forcing in 12r1 has less important impact on seasonal time-scale integrations compared to the impact arising from the changes to the model formulation.

For each model cycle considered, the model climate was computed from the average of all 15 experiments. Only the last three months, corresponding to the conventional winter calendar season, were analysed. The ensemble (seasonal) averages were computed from seasonal averages of respective individual experiments. For verification purposes the observed (ensemble) seasonal averages were also calculated.

The changes to the parametrization of soil processes in CY48 made obsolete the use of deep climatological soil-moisture and soil-temperature fields. However, no re-assimilation for the initial data has been done; the initial data for CY48 and 12r1 were obtained from operationally archived data using standard ECMWF procedures.

4. Model climate drift in upper air fields

4.1. Wintertime circulation

Fig.1 shows the ensemble averages of 500 mb geopotential height for the DJF season. In addition to the mean model and analysis fields, a long-term ECMWF climate is also shown (Fig.1f). All model cycles reproduce with reasonable accuracy the main features of the northern hemisphere wintertime circulation. However, a more detailed analysis of the simulated flow allows a clear distinction between different model versions. In the CY48 map (Fig.1c), a stronger and more realistic ridging is seen over the Alaskan region than in CY36 and CY46. Whereas in the two earlier model cycles the Pacific jet extends too far east (thus indicating too strong zonal flow), in CY48 a weaker north-south gradient over the eastern Pacific is associated with an enhanced diffluence and a stronger northerly flow component downstream into the North American mainland. In 12r1, the ridging over the far east Siberia, near the date line, is quite realistic and the meridional gradient in the eastern Pacific is weakened even further.

Over the eastern Atlantic, the intensification of the westerly flow still takes place; the diffluence over the Atlantic-European region in CY48 is similar to the diffluence in the two earlier model cycles and is weaker than observed. In 12r1, the Canadian Arctic low is somewhat deeper than in the other models and analysis. This deepening is associated with a weakened ridging in the north Atlantic and a stronger than observed model jet over the western and central Atlantic (see also discussion in section 4.4).

The model climate drift (simulated ensemble-mean minus observed mean) maps for 500 mb height in the northern hemisphere and southern hemisphere are shown in Fig.2. In the northern hemisphere, the error pattern and error amplitude in CY36 and CY46 are very similar (Fig.2 a and b). A strong positive-negative error dipole over the northern Pacific-Alaskan region, which indicates a model tendency to smooth out planetary-scale waves, is greatly reduced in CY48 (Fig.2c) and further reduced in 12r1 (Fig.2d). Over the eastern Atlantic-European region, the trough-to-ridge amplitude of the error dipole is slightly weaker in CY48 relative to the earlier cycles, and the gradient in the error field between Iceland and the western Mediterranean is weakened as well. This error dipole has been strengthened in 12r1, thus indicating an Atlantic jet stronger than in the analysis.

In the southern hemisphere, a different model behaviour is found (Fig.2 e-h). A large reduction in climate drift is seen from CY36 to CY46. The error pattern in Fig.2e indicates that CY36 overestimates the circumpolar vortex (also discussed by Branković and Ferranti, 1992). CY46 makes this vortex more realistic, while both CY48 and 12r1 show a tendency to further decelerate the southern circulation so that it is underestimated in these two cycles. In CY46 and CY48 a weak negative geopotential height error dominates in low latitudes and is slightly more negative in 12r1. A possible explanation why CY46 makes an improvement over CY36 in the southern but not simultaneously in the northern hemisphere might be in the fact that the impact of the revised cloud shortwave optical properties introduced with CY46 is strongly seasonally dependent, i.e. their beneficial impact is primarily seen in the summer hemisphere over the high-latitude region with semi-permanent daylight. However, other changes introduced between CY36 and CY46 may have contributed to such an improvement as well.

Hemispheric differences in the error pattern at 1000 mb (not shown) are similar to those at 500 mb. In the northern hemisphere, the main improvement in CY48 comes from a better representation of the subtropical high between the Hawaiian Islands and the western coast of North America. In CY36 and CY46 this high was overestimated, displacing the Aleutian low too far north and causing strong surface westerlies over the northeastern Pacific. Despite the fact that the Atlantic subtropical high is better simulated in 12r1 than in the other cycles, the north Atlantic/European surface westerlies are found to be overestimated. This is mainly due to a somewhat too deep Icelandic low in 12r1.

In contrast to the middle and lower troposphere, a somewhat different change of model drift is seen in the upper troposphere. At 200 mb, the northern hemisphere high latitude negative height error (not shown) remains almost unchanged for CY36, CY46 and CY48 in both pattern and amplitude. In 12r1, this error has been reduced over the north Pacific, but slightly increased in the north Atlantic, thus being consistent with the cycle 12r1 errors in the middle and lower troposphere. In the southern hemisphere, CY36 errors, which are similar to those in Fig.2e, are replaced in CY46 by a negative error, dominating over the entire hemisphere. CY48 exhibits further reduction of this

negative error, whilst in 12r1 the upper troposphere error is rather small (see also section 4.2 on temperature errors).

Additional discussion on model mean height errors is given in section 7.2.

The error structure in zonally averaged zonal wind (Fig.3) is consistent with the height error pattern discussed above. In the northern hemisphere in all cycles, a positive u-wind error north of 30°N, and a negative error in the subtropics and tropics, are mainly a consequence of poleward displacement of the wind maximum relative to the analysis. Although the a northward shift is seen in all model cycles, it is smallest in 12r1. In both CY48 and 12r1 the northern hemisphere westerly error is confined to the upper troposphere and lower stratosphere. However, in cycle 12r1, the polar night jet near the top of the model is too strong and consequently the westerly error is larger than in the other cycles. A relatively large negative error in the tropics at the tropopause level in CY46 (Fig.3c) accounts, in addition to the jet poleward shift, for too strong tropical easterlies (seen to a much lesser degree in the other three model cycles).

In the southern hemisphere, a large westerly error in CY36 is, similar to the northern hemisphere, a consequence of both strengthening of zonal wind and its poleward displacement. In all later model cycles this error is greatly reduced and reflects the progressive deceleration of the circumpolar vortex with each cycle (see also Fig.2 e-h).

The error in the model eddy kinetic energy is gradually reduced with each cycle, especially in the tropical upper troposphere and lower stratosphere (Fig.4). A large positive error in eddy kinetic energy in the southern hemisphere midlatitudes in CY36 is very likely associated with large error in zonally averaged circulation (Fig.3b).

4.2 Temperature errors

The error pattern in zonally averaged temperature has been substantially changed from one model cycle to the other (Fig.5). In the model tropical upper atmosphere, a very small error in CY36 (Fig.5a), is modified to relatively large errors in CY46 , alternating in sign with height (Fig.5b). Such an error pattern, but with somewhat reduced amplitude is also found in CY48 (Fig.5c), while in 12r1 (Fig.5d) the warming of the model tropical upper atmosphere reaches as much as 5°K. It seems plausible to ascribe these errors to the changes in radiation and cloud parametrization introduced with CY46. Indeed, a similar error pattern in the tropical stratosphere as in Figs.5b to 5d is seen at mean forecast day 10 (D10) for March 1993 ECMWF operational forecasts (not shown). In January 1993, i.e. prior the introduction of the CY46 changes, D10 upper atmosphere temperature error pattern was different from that in Fig.5b with a weak cooling throughout the tropical upper troposphere and lower stratosphere.

In Fig.5 in the polar stratosphere of both hemispheres, a large negative temperature error is seen, the error being larger in the summer hemisphere. While the erroneous cooling in the northern hemisphere is almost unchanged in various model cycles, in the southern hemisphere it has been reduced by about 7°K (or nearly 50%) from CY36 to 12r1. This polar stratospheric cooling is a common feature of many GCMs and its origin is not well understood (Boer *et al.* 1991). Lary and Balluch (1993) suggested that taking into account the effects of spherical geometry in the parametrization of radiation processes (rather than the plane parallel approximation used by almost all GCMs) would significantly reduce the underestimation of the solar heating rate, especially in polar regions. However, in the case of the ECMWF model, the changes to the formulation of physical parametrization are partly responsible for the reduction of this error from CY46 to 12r1. Some of the beneficial impact seen in the cycle 12r1 polar stratospheric temperature error may have come from the improved vertical resolution in this model cycle. This is suggested by comparing zonally averaged temperature errors in the medium-range for the 19-level T63 control (unperturbed) forecasts from the Ensemble Prediction System against 31-level operational T213 forecasts. The 19-level model has stronger cooling in the DJF southern polar stratosphere than 31-level model.

4.3 Mean meridional circulation

For reasons of space, mean meridional circulation comprising of zonally averaged vertical and meridional velocities will be discussed without displaying figures.

In successive model cycles, the intensity of the DJF lower tropospheric large scale ascent (centred in the analysis at about 5°N and mainly associated with the Pacific intertropical convergence zone, ITCZ), is progressively increased and its positioning is shifted slightly northwards. This increase varies between about 15% relative to analysis in CY46 to over than 70% in 12r1. (Note, however, that the operational analysis itself may be deficient in this respect, since it was performed using much earlier cycles of the forecast model.) At the same time, the intensity of the upper tropospheric ascent at about 10°S, that can be associated with the south Pacific convergence zone (SPCZ), and the intensity of the descending branch of the Hadley cell between 15 and 20°N do not change significantly in the model (apart from CY46 where the upper air ascent is much weaker than in the other models and analysis). Thus the strengthening of the vertical circulation in the Hadley cell, seen especially in CY48 and 12r1, is primarily due to the enhancement of rainfall within the Pacific ITCZ (cf. section 5).

The outflow branch of the zonally averaged meridional wind is weakest in CY46, but is steadily increasing in the later cycles thus indicating an overall strengthening of the Hadley circulation. It is interesting to note that, when compared with the analysis, all model cycles show a strengthening of the thermally indirect Ferrel cell, being the strongest in CY36. This is associated with an increased eddy momentum flux convergence in the model, which in turn is associated with

an overall enhancement in eddy momentum flux (not shown). Such an increase is most pronounced in CY36, where the eddy momentum flux error in the southern hemisphere middle latitudes amounts to about 50% of the observed maximum.

4.4 The largest differences between successive cycles

In this section we focus on some of the DJF ensemble mean difference fields between CY48 and CY46, because they were found to be the largest differences between cycles. As indicated in section 2 and Table 1, CY46 changes were related to the cloud and radiation parametrization, whereas CY48 changes were mainly in the parametrization of soil processes and PBL.

Fig.6 indicates a relative change from CY46 to CY48 for 500 mb height, 850 mb temperature and 850 mb relative humidity. The enhanced ridging over the Alaskan region in CY48 is seen as a positive difference in Fig.6a. This positive difference extends throughout northern polar latitudes, thus implying an overall increase of geopotential height in CY48. Over the Canadian Arctic, this increase results in a more realistic semi-permanent low, which was too deep in CY46. However, over northwestern Siberia, this positive difference implies a weaker trough, which in turn contributes to a weakening of the wavenumber 3 pattern in high latitudes (cf. observed circulation shown in Fig.1e).

Negative differences over the northern Pacific are indicative of a more realistic trough-ridge system over the eastern Pacific/Alaskan region in CY48. However, the extension of these negative differences into eastern Asia indicates a deepening of the trough over the Kamchatka peninsula and strengthening of the jet off the coast of Japan. Negative differences over much of North America indicate a more realistic simulation of the trough over the eastern U.S. with CY48.

For 850 mb temperature (Fig.6b), the difference pattern between CY48 and CY46 over the north Pacific/Alaskan region is consistent with the height differences in Fig.6a. The cooling over the north Pacific is not necessarily a deficiency of CY48. According to the ECMWF re-analysis project experimentation, the analysis based on model cycle 48 (which fits observations better), would be cooler over the north Pacific in comparison with analysis based on model cycle 46 (Per Kållberg, personal communication). Thus, negative temperature differences seen over much of the north Pacific would imply a reduced climate drift in CY48 with respect to an improved analysis.

A striking feature in Fig.6b is a warming of tropical and subtropical continents in CY48, with maxima in the tropical South America and Africa exceeding 4 degrees. Closely related to such a difference pattern is drying over the same regions (Fig.6c). Because of its confinement to the land points, it seems likely that the cause for such a difference pattern is the new scheme for soil processes rather than the other changes introduced with CY48.

A large change in relative humidity at 850 mb over the oceans in Fig.6c can be, on the other hand, attributed to a small but significant increase in the height of PBL. The entrainment at the top of PBL, introduced with CY48, makes (on average) the model PBL deeper relative to the depth of PBL in the previous cycles. The pressure level of 850 mb is (because of its proximity to the top of PBL) on average more frequently below the inversion level rather than in the drier air above.

The tropical upper troposphere geopotential height significantly decreased from CY36 to CY46 (Fig.7a). This remarkable decrease on the tropical planetary scale is most likely associated with much weakened Hadley circulation in CY46 as discussed above. With the introduction of CY48 the tropical heights recover (Fig.7b), with the tendency to further increase in 12r1 (Fig.7c).

5. Precipitation

The zonally averaged total rainfall amounts for the four model cycles and for the DJF climate (Legates and Willmott 1990) are shown in Fig.8a. Over much of the globe there is a broad agreement between the cycles studied here. The main difference is the larger tropical precipitation in CY48 and 12r1 than in the two earlier cycles, particularly at 10°N and 10°S which corresponds to the ITCZ and the SPCZ respectively. The largest contribution to such an increase comes from convective precipitation over the oceans (Fig.8b), which may be attributed to the modification in the parametrization of shallow convection (see section 2 and Table 1). All models show a northward displacement of the ITCZ rainfall relative to the DJF climate. Despite the shift, the later two model cycles undoubtedly represent an improvement over the former two cycles. However, the minimum at the equator is too deep in the model.

In the extratropics, CY36 is the wettest of the four. The largest difference is again due primarily to convective precipitation over the oceans, since the contribution from the large-scale precipitation to total amounts is very similar in all four cycles (not shown). In both hemispheres between 50° and 60°, for example, CY36 convective precipitation is almost twice as large as CY48 (Fig.8b). In the southern hemisphere storm track (around 60°S), the climate maximum greatly exceeds the model values. A similar result is found when the Jaeger (1976) climate is used as the reference, in spite the fact that the latter is systematically dryer than the Legates and Willmott data. Even if the simulated southern hemisphere rainfall amounts are taken as a serious model deficiency, the discrepancy between the model and observed climatologies is so large that one may question the reliability of the observed climate data. Both rainfall climatologies are subject to high uncertainties in the southern hemisphere mid-latitudes because of large data void areas.

The global distribution of the DJF rainfall in the model cycles and for the DJF climate is shown in Fig.9. One sees clearly the intensification of the Pacific ITCZ and SPCZ in CY48 and 12r1 relative to the other two cycles. The Atlantic ITCZ off South America has intensified as well. The

ITCZ double structure in the Indian Ocean which straddles the equator in CY46 becomes a broader structure with larger rainfall amounts in the later two cycles. The Australian rainfall is, apart from CY36, confined to the northern (monsoon rainfall) and eastern parts of the continent. This may be associated with the use of the new climatological albedo field which has a somewhat higher values over Australia in comparison to that used in CY36. Another marked change in the rainfall pattern is found over the Amazon basin immediately to the south of the equator. Both CY48 and 12r1 exhibit there much reduced rainfall amounts compared with CY46. In contrast, over south Africa they produce more rain than CY46.

In the extratropics, differences between the model cycles are relatively small, both in amplitude and spatial coverage. Along the northern storm tracks, a somewhat less rain is found in CY48 than in the other three cycles. In the southern hemisphere storm track, CY36 has more rain than the other cycles (see Fig.8).

The main differences between model and climate (Fig.9e) precipitation fields may be summarized as follows. In the model, regardless of the cycle, the Pacific ITCZ is represented by a relatively narrow band of rainfall and elongated maximum, while in the climate the ITCZ is wider with a well defined rainfall maximum at about 140°W. However, an elongated ITCZ rainfall maximum in observed data, similar to that seen in the model but with a weaker amplitude, is found by Dorman and Bourke (1979).

The climatological Indonesian maximum is much higher than any of the simulated ones; in the model it is characterized by "spotty" maxima scattered over Indonesian and Philippine islands with (too low) rainfall minima between them. It could be said that the simulated rainfall pattern over this region is dominated by orographic features. The influence of orography is even more pronounced in the model rainfall amplitude and pattern over Central and South America. The Indian Ocean ITCZ in the model is more intense than that in the climate data. In the extratropics, the climate has somewhat more rainfall than the model in both northern storm tracks; in the southern hemisphere the modelled precipitation rate is very much underestimated (see also discussion above).

6. Circulation regime statistics

6.1 Frequency of blocking

Fig.10 shows frequency of blocking occurrence, as defined by Tibaldi and Molteni (1990), averaged over the five winters of experimentation. The analysed frequency (dashed line) has two main maxima, one over the Atlantic/European region and another over the eastern Pacific. In all four model cycles, the amplitude of the Atlantic maximum is relatively close to the observed value, but

its position is displaced eastward. This eastward model bias suggests that the mean flow pattern over the central and eastern Atlantic has changed very little from one model cycle to the next; the Atlantic jet is still overestimated in the model and penetrates too far east, thus shifting the region of upper-air diffluence into the European continent (cf. Fig.1). A relative improvement in CY48 and 12r1 is seen further east where the location of the secondary maximum at 60°E (the Ural mountains) is reasonably well captured in 12r1, but has much overestimated amplitude in CY48. In 12r1, in addition to the eastward shift, the Atlantic maximum has been weakened relative to the analysis and to the other cycles. This deterioration in the representation of blocking frequency can be associated with the strengthening of the Atlantic jet as discussed in section 4.1.

Over the Pacific region CY36 and CY46 substantially underestimate frequency of blocking occurrence. This deficiency is somewhat alleviated with CY48. In view of the discussion in section 4.1, this improvement should be associated with a better representation of the 500 mb ridge in the northern Pacific/Alaskan region and the reduction of the model climate drift in CY48. We note that in their famous study of the 1977 winter, Miyakoda *et al.* (1983) showed that sensitivity of their model to the treatment of PBL was critical for a successful simulation of the Pacific blocking event. Further reduction of the model mean error over the north Pacific seen in Fig.2d, together with a realistic low-frequency variability (not shown) reflect as substantial improvement in the representation of blocking in 12r1 (Fig.10d).

A simple argument based on a study by Ferranti *et al.* (1994b) may explain why CY48 and particularly 12r1 show an improvement in frequency of blocking over the north Pacific. Based on experimental evidence, they found that the strongest impact on the modelled blocking activity in both Pacific and Atlantic/European regions was due to an increase of quasi-stationary diabatic heating over the western tropical Pacific. Such an increase in diabatic heating was introduced into their experiments via an idealized strong positive SST anomaly defined in the Indonesian region, which is manifested in the model as an increase in rainfall over the western tropical Pacific.

The difference in the rainfall between 12r1 and CY36 in the western Pacific is shown in Fig.11. A relatively large and coherent area of positive differences exceeding 4 mm/day is found over much of the western Pacific (including Borneo, southern part of the South China Sea, the Philippines and Papua/New Guinea). This increase in the 12r1 rainfall amount may be viewed as an equivalent to the increase in diabatic heating in Ferranti *et al.* study. However, unlike to their experiments, this increase cannot be linked to changes in the local SST forcing, since the SST fields in CY36 and 12r1 were essentially identical. Therefore, an increase in 12r1 rainfall over Indonesia must be attributed to an improved model efficiency in exploiting existing SST forcing. The result in Fig.11 shows a cumulative effect of all the modifications introduced between CY36 and 12r1, and the rainfall increase shown in Fig.11 should not be ascribed to the 12r1 changes alone.

6.2 Planetary-wave regimes

The ability of the different model cycles to reproduce low-frequency variability in the planetary-scale flow is tested by evaluating the frequency of occurrence of the five main regimes of 500 mb planetary waves defined by Molteni *et al.* (1990) from a 32-winter record of 500 mb height analyses. The regimes were defined as clusters associated with local maxima in the probability distribution of the projections of eddy fields onto three rotated empirical orthogonal functions (REOFs). Following Ferranti *et al.* (1994a), the projections onto these three REOFs have been computed using running 5-day mean anomalies from the 15 model integrations, and each field has been classified in one particular cluster according to the distance between its position in the 3-dimensional REOF space and the position of the centroids of the clusters (the closest centroid has been selected).

A similar classification has been performed on ECMWF analyses from winter 1979/80 to 1990/91; the model frequency will be compared with the observed frequencies in either this 12-winter sample or in a shorter sample including only the five winters, i.e. those corresponding to the initial dates of the experiments. (Given the simpler classification method used here, a comparison with the long-term climatological frequencies from Molteni *et al.* 1990 is not appropriate). In evaluating these results, we remind the reader that clusters 1 and 2 correspond to anomalies with positive Pacific/North American (PNA) index, clusters 3 and 5 to anomalies with negative PNA index. Clusters 2, 4 and 5 represent flows with larger-than-average planetary wave amplitude, while cluster 1 (the most populated) includes fields which are fairly close to the climatological mean state.

The comparison between the modelled frequencies and the observed frequencies is shown in Fig.12. For each cluster, the modelled frequencies are shown as the left-hand bars, the 5-year observed frequencies as the centre bars and the 12-year observed frequencies as the right-hand bars in Fig.12. When compared with the 5-year frequencies in all four model cycles, the frequencies of positive-PNA clusters (1 and 2) are overestimated, while those of clusters 3 and 4 are underestimated. Overall, the bias towards clusters 1 and 2 is larger in CY48 and in 12r1 than in the previous cycles; indeed, both CY48 and 12r1 underestimate (the former significantly and the latter slightly) the frequency of cluster 5 with respect to the 5-year analysis, which the previous cycles did not. The large frequency of cluster 2 in CY48 is consistent with the strengthening of the ridge over the Rockies documented above.

However, if one uses the 12-winter analysis sample as a comparison (the right-hand bars in Fig.12), one notices a better agreement between observed and modelled frequencies for all cycles, and CY48 turns out to give the best results, followed closely by CY36 and 12r1. One can argue that, since cluster frequencies are subject to considerable sampling errors, the 12-winter sample gives a more sound basis of comparison that the 5-winter one. On the other hand, the 12-winter

sample includes the very strong El Niño event of 1982/83, while no cold event of comparable intensity to the 1988/89 La Niña is present. Consequently, the 12-winter sample is more "biased" towards positive PNA anomalies, and this may compensate for model systematic errors. Insofar as the differences between the 12-winter and the 5-winter samples are a real reflection of differences in the boundary forcing, one cannot conclude that CY48 or 12r1 represent an improvement with respect to CY36 in the simulation of large-scale regimes. This will be confirmed by the discussion on interannual variability in the following section.

7. Simulation of interannual variability

7.1 Differences between two strong ENSO winters

The impact of different model formulations on simulation of interannual variability is discussed first in terms of the modelled differences between two strong ENSO index winters, DJF 1986/87 and DJF 1988/89. The former was an El Niño year with a strong positive SST anomaly in the equatorial Pacific; the latter was a La Niña year with a strong negative Pacific SST anomaly (see Branković *et al.* 1994, for a description of the SST anomalies in the period 1986 to 1990).

a. Tropical Pacific

The difference in response of the 200 mb vector wind to those strong differences in SST forcing in the tropical Pacific is presented in Fig.13. In the analysis (Fig.13a), the central Pacific wind differences resemble the flow anomaly obtained in the Gill (1980) linear model when forced with a low-level equatorial heating. On either side of the equator a pair of closed anticyclonic circulations is clearly seen, associated with relatively strong easterlies along the equator. The large magnitude of the Pacific differential circulation in Fig.13a reflects the differences in the two anomaly fields driven by a relative strong SST forcing of the opposite sign. The cyclonic curvature further north in the northern Pacific is indicative of negative geopotential differences, part of a broader PNA teleconnection wavetrain pattern.

In the model ensemble averages, both the shape and intensity of the Pacific differential circulation are captured reasonably well with all cycles except CY46, indicating a correct model response to the low-level heating anomalies. This circulation is very much underestimated in CY46. Both CY48 and 12r1 produce realistic equatorial easterlies and differential circulation south of the equator. CY36 produces more realistic differences in the northern subtropical Pacific, particularly southerly wind differences between 150°E and 180° and cyclonic curvature along 30°N. In all cycles but CY46, the westerly differential flow off the South America western coast is overestimated, and extends too far across the South American continent into the Atlantic.

At 850 mb, over the tropical Pacific, the westerly differences are dominant, i.e. of the opposite sign to those aloft (not shown). This feature is well represented in the model, but with too strong a magnitude, especially in CY36. This may be interpreted as the tendency of the model to enhance the 850 mb divergence (or reduce convergence) in the western Pacific. The weakest wind differences are again found in CY46.

b. Northern extratropics

The response of the northern extratropical atmosphere to the strong differences in the equatorial Pacific SST forcing in winters of 1986/87 and 1988/89 is discussed in terms of 500 mb height differences (Fig.14). In the analysis (Fig.14e), the wavetrain structure extends from the tropical Pacific, over North America, into the tropical Atlantic. Such a wavetrain is typical of a positive PNA teleconnection pattern as described in, for example, Horrel and Wallace (1981). In addition, two further centres are seen: positive in the north Atlantic, between Greenland and Iceland, and negative over Europe. Similarly to the wind field, the height differences are of much larger amplitude than in standard anomaly fields for individual seasons (cf. Fig.16a).

The model simulated, ensemble mean height differences between the two winters are shown in Fig.14 a to d. Apart from CY46, a well established wavetrain over the PNA region, similar to that in the analysis, is seen for the other model cycles. The North American maximum and the adjacent oceanic minima are well located in CY36 and 12r1 when compared with the analysis, but displaced westward in CY48. On the other hand, CY48 as well as 12r1 represent well the negative differences over Europe, which are underestimated in CY36. In CY36 and CY48, amplitudes of differences over the PNA region are somewhat weaker than the analysed ones, while in 12r1 they are quite realistic. It has to be borne in mind that weaker amplitudes in an ensemble mean may reflect the smoothing due to averaging of three model realizations for a relatively chaotic extratropical atmosphere.

The CY46 representation of interannual variation for 500 mb heights is very poor (Fig.14b). The amplitude of differences is much smaller than in the other three model cycles. A major deficiency is the almost complete absence of the north Pacific minimum. The North American maximum is also much weaker and confined to the Alaskan region; thus no characteristic PNA wavetrain pattern in CY46 can be seen.

Another way to assess the ability of the model to represent interannual variability is to compare the difference in the frequency of atmospheric large-scale regimes between the El Niño and the La Niña winters. For this purpose, the five planetary-wave clusters discussed in section 6.2 will be used. The observed cluster frequencies in these two winters are shown in Fig.15a (with DJF 1986/87 on the left in each pair). Although sampling problems certainly affect individual winter estimates, the predominance of the positive-PNA cluster 1 in 1986/87 and of negative-PNA clusters

(3 and 5) in 1988/89 is clear in Fig.15a, and is consistent with well-documented relationships between SST and extratropical flow anomalies.

The cluster frequencies in these two winters from the four model cycles are shown in Fig.15 b to e. Cycle 12r1 shows the clearest shift from positive to negative PNA clusters when going from 1986/87 to 1988/89, while CY36 shows a similar but weaker signal (as already documented in Branković *et al.* 1994). For CY48 the cluster differences are small, probably within sampling errors, while for CY46 the signal seems to be opposite to the observed one.

As discussed in section 6.2, the frequency of planetary-scale clusters is very sensitive to sampling. To demonstrate this further, we compare the results from the two CY36 ensembles of distinctly different size: the original 3-member ensembles and extended 9-member ensembles. (The latter were discussed extensively by Branković and Palmer 1996). For the 3-member CY36 (Fig.15b), one should point out that the differences between the two winters are concentrated in the two clusters with large wave amplitude (clusters 2 and 5), while the impact on cluster 1 (which was large in the analyses) is smaller and actually opposite to the observed one. However, we can show that this result is just due to poor sampling. Fig.15f again refers to CY36, but the modelled frequencies are computed from 9 experiments for each winters (this extended dataset is only available for CY36). One can see that impact on cluster 1 frequency is now in agreement with the observations, while the overestimation of cluster 2 is reduced. This confirms the importance of large ensembles for the assessment of the statistical properties of low-frequency variability in the model.

7.2 Model errors in two strong ENSO winters

In this subsection we investigate the relationship between model simulated interannual variability for seasons DJF 1986/87 and DJF 1988/89, discussed above, and model mean errors. This is carried out for CY36, CY48 and 12r1, because, as inferred from Fig.14, these model versions give better representation of northern hemisphere interannual variation than CY46. Ideally, the model error in each year representing strong interannual variation should be small, and the error pattern should be insensitive to the observed anomaly.

Fig.16a,b shows observed 500 mb height anomalies for DJF 1986/87 and DJF 1988/89 respectively. The relatively large amplitudes and the opposite sign of anomalies over the PNA and Atlantic/European regions are typical of mid-latitude atmospheric response to a strong and opposite equatorial Pacific SST anomaly forcing.

CY36 ensemble mean errors in both winters are very similar (Fig.16c,d). Some differences in the amplitude of errors are seen, however, the basic error pattern is common to both winters: a positive error over the northern Pacific, a negative error over the Alaskan region and positive again over the eastern coast of North America. In the La Niña winter (Fig.16d), due to a stronger negative

error over Alaska, the Atlantic/European error dipole is shifted southeastward. The occurrence of large and similar errors in these two winters, despite different SST anomaly boundary forcing, is indicative of a strong systematic bias in CY36.

On the other hand, the CY48 errors (Fig.16e,f) over the PNA region in DJF 1986/87 are different from those in DJF 1988/89. Positive error over the north Pacific in the El Niño winter (where the observed anomaly is negative) is replaced with a relative strong negative error in the La Niña winter (when the observed anomaly is positive). Again, over the eastern part of North America errors in these two winters are of the opposite sign (and opposite to the observed anomalies). Overall, the mean error pattern in CY48 behaves less systematically in comparison with CY36.

The fact that CY48 errors over much of the northern hemisphere are almost opposite to observed anomalies would imply that, on a longer time scales, CY48 tends to counteract the effect of the observed anomalous circulation. In contrast to CY36, CY48 errors have become more dependent on the flow type.

Though the cycle 12r1 errors (Fig.16g,h) may appear similar to those of CY48, the main differences are as the following. The 12r1 error amplitudes are larger than in CY48 over the Atlantic/European and Asian regions in the El Niño winter and smaller (over the same regions) in the La Niña winter. A detailed inspection of Fig.16g,h indicates a slight eastward shift in the positioning of the PNA error centres in 12r1 relative to CY48. This different location of the major error centres in 12r1, together with a weak negative error just to the north of the Hawaii Islands (Fig.16g), seem to have played an important role in a relatively successful representation of interannual variability by 12r1 as shown in Fig.14d.

The above discussion is further supported by the 500 mb height correlation coefficients between observed anomalies and model errors for the two winters. These are shown in Table 2 for the PNA and Atlantic/European regions. (The regions' boundaries are identical to those defined in Branković *et al.* 1994.) If the model error pattern was identical to the observed anomaly pattern and of the opposite sign, the correlation coefficient would be exactly -1. Table 2 shows that in both winters, CY48 has the strongest tendency to counteract observed anomalies, consistent with the discussion above. 12r1 seems to be superior to CY36 because, on average, it has weaker correlations than CY36.

8. Summary and conclusions

Four different versions (cycles) of the ECMWF NWP model have been integrated at low (T63) resolution on the seasonal time scale in order to study the influence of various model formulations on model climate. The model versions, denoted as cycles 36, 46, 48 and 12r1, differ primarily in

the representation of physical processes, but in cycle 12r1 a higher vertical resolution was also used for technical reasons. The successive cycles were introduced in ECMWF operations over the period of about four years, from 1990 to 1994.

For five northern winter seasons (DJF 1986/87 to 1990/91) three 120-day experiments, initiated from initial data one day apart, were run for each model cycle. The four model climatologies were derived as averages of 15 integrations in each cycle. In the first three cycles the observed SST was updated every five days throughout the experiment integration, but was updated daily in cycle 12r1.

With the introduction of cycle 48, an apparent improvement in the northern hemisphere wintertime climate of ECMWF model has been observed. A strong systematic bias in the earlier cycles in the northern hemisphere, associated with an overestimation of the zonal flow in the eastern Pacific and a weak diffluence over western North America, was reduced and replaced by more realistic ridging over the north Pacific/Alaskan region. This error has been further reduced in cycle 12r1. The improvement is associated with a reduction in the temperature error over the northeastern Pacific. A reduction of errors in zonally averaged zonal wind and eddy kinetic energy is also evident.

While cycle 46 has a reduced model climate drift in the southern hemisphere summer, its contribution to the northern hemisphere winter mean flow is not evident. It was argued that the impact of the revised cloud shortwave optical properties introduced with cycle 46 is strongly susceptible to seasonal forcing. However, other model changes introduced between cycle 36 and cycle 46 may also have contributed to the reduction of the southern hemisphere climate drift.

The frequency of blocking with cycle 12r1 is much more realistic over the north Pacific region when compared with the other three cycles, though it was slightly improved already in cycle 48. It was argued that this improved representation of the northern Pacific block is due to more efficient diabatic response to the warm SSTs over the Indonesian region. A slight deterioration of blocking frequency in cycle 12r1 over the Atlantic/European region is associated with the strengthening of the Atlantic jet in comparison with the other cycles.

Not all parameters exhibited an improvement in the climate drift in successive cycles. For example, in the lower troposphere a negative temperature error has slightly increased over the oceans from cycle 46 to cycle 48, and the tropical continents have become too warm. The former is associated with an increase in the lower tropospheric humidity in cycle 48 relative to cycle 46. This is the consequence of a small increase in the height of PBL in cycle 48, which in turn is due to the introduction of entrainment at the top of PBL. On the other hand, a relative warming over the tropical continents implies further drying and larger errors in cycles 48 and 12r1. A strong polar stratospheric cooling in both hemispheres is still seen in cycle 12r1, however, this has been greatly

reduced in the southern (summer) hemisphere. A warming of the tropical lower stratosphere, which became apparent with the introduction of cycle 46, is still very much evident in cycle 12r1. This error is not unique to seasonal integrations - it has been also seen in the ECMWF operational medium-range forecasts.

The Hadley circulation, which was somewhat weakened from cycle 36 to cycle 46, has become more intense again with the later cycles. However, the lower branch of the large-scale tropical ascent is now overestimated when compared with the operational analysis (which is likely to be deficient in this respect). This is associated with an intensification in convective rainfall within the tropical convergence zones in cycles 48 and 12r1, particularly over the Pacific. This in turn may be attributed to a more active shallow convection in these cycles. Another prominent feature of the later cycles is the concentration of tropical precipitation into relatively narrow bands that represent the main tropical convergence zones. Lack of observations to provide climatological data makes the verification of the southern hemisphere model precipitation uncertain.

In terms of representing the northern hemisphere circulation, model cycles 36 and 46 are comparable and cycles 48 and 12r1 can be regarded as improvements over the former two cycles. Cycle 36 has a relatively strong systematic bias which is insensitive to observed anomalies in winters of 1986/87 and 1988/89. In simulating interannual variability for the two strong and opposite ENSO-index winters, cycle 46 is the least successful. This interannual variation seems to be most realistically represented with cycle 12r1. The relatively small climate drift in cycle 48 is explained by a partial offset between model mean errors and observed anomalies in strong and opposite ENSO years. In other words, the bias in cycle 48 is more flow dependent and less "systematic" than in cycle 36. Such a model behaviour requires a cautious interpretation of the model representation of interannual variation in the presence of strong and opposite SST forcing (see also Mo and Wang 1995).

Verifications of modelled low-frequency variability in terms of frequency of the north hemisphere flow regimes indicate a reasonable similarity between observed and modelled frequencies for all cycles when results from the whole set of experiments are compared with the observed 5-year and 12-year data. When the 12-year sample is used as a reference, cycle 48 has the best performance, closely followed by cycle 12r1. However, the interannual variability of cluster frequencies between opposite ENSO phases is reproduced most satisfactorily by cycle 12r1.

Overall, the most recent ECMWF model versions, cycle 48 and especially cycle 12r1, have generally a better wintertime climatology than earlier versions. On seasonal time scales, some of the model systematic errors have been steadily reduced and model's ability to reproduce interannual variations has been improved. However, despite considerable improvements, there are still deficiencies in the model climate which warrant further efforts to eliminate them.

Acknowledgments: We thank Mike Blackburn, Tony Hollingsworth, Martin Miller, Jean-Jacques Morcrette, Tim Palmer and Adrian Simmons for constructive discussions and valuable comments on earlier version of the paper.

References

Boer, G.J., K.Arpe, M.Blackburn, M.Déqué, W.L.Gates, T.L.Hart, H.le Treut, E.Rockner, D.A.Sheinin, I.Simmonds, R.N.B.Smith, T.Tokioka, R.T.Wetherald and D.Williamson, 1991: An intercomparison of the climates simulated by 14 atmospheric general circulation models. CAS/JSC Working Group on Numerical Experimentation. Report No.15, WMO/TD-No.425.

Branković, Č. and L.Ferranti, 1992: Seasonal integrations with realistic boundary forcing. Pp 305-333 in Proceedings of the ECMWF Workshop "New Developments in Predictability". ECMWF, Shinfield Park, Reading, UK, 13-15 November 1991.

Branković, Č. and T.N.Palmer, 1996: Estimates of atmospheric seasonal predictability in ensemble integrations. *Mon.Wea.Rev.* (submitted)

Branković, Č., T.N.Palmer and L.Ferranti, 1994: Predictability of seasonal atmospheric variations. *J.Climate*, **7**, 217-237.

Dorman, C.E. and R.H.Bourke, 1979: Precipitation over the Pacific Ocean, 30°S to 60°N. *Mon.Wea.Rev.*, **107**, 896-910.

Ferranti, L., F.Molteni, Č.Branković and T.N.Palmer, 1994a: Diagnosis of extra-tropical variability in seasonal integrations of the ECMWF model. *J.Climate*, **7**, 849-868.

Ferranti, L., F.Molteni and T.N.Palmer, 1994b: Impact of localized tropical and extratropical SST anomalies in ensembles of seasonal GCM integrations. *Q.J.R.Meteorol.Soc.*, **120**, 1613-1645.

Gill, A.E., 1980: Some simple solutions for heat-induced tropical circulations. *Q.J.R.Meteorol.Soc.*, **106**, 447-462.

Horrel, J.D. and J.M.Wallace, 1981: Planetary-scale atmospheric phenomena associated with southern oscillation. *Mon.Wea.Rev.*, **109**, 813-829.

Hurrell, J.W., 1995: Comparison of NCAR Community Climate Model (CCM) climates. *Climate Dynamics*, **11**, 25-50.

Jaeger, L., 1976: Monatskarten des Niederschlags für die ganze Erde. Berichte des Deutschen Wetterdienstes, **139**, Band 18.

Lary, D.J. and M.Balluch, 1993: Solar heating rates: the importance of spherical geometry. *J.Atmos.Sci.*, **50**, 3983-3993.

Legates, D.R. and C.J.Willmott, 1990: Mean seasonal and spatial variability in gauge-corrected, global precipitation. *Int. J. Climatol.*, **10**, 111-127.

Miller, M.J., A.C.M.Beljaars and T.N.Palmer, 1992: The sensitivity of the ECMWF model to parametrization of evaporation from the tropical oceans. *J.Climate*, **5**, 418-434.

Miyakoda, K., T.Gordon, R.Caverly, W.Stern and J.Sirutis, 1983: Simulation of blocking event in January 1977. *Mon.Wea.Rev.*, **111**, 846-869.

Mo, K.C. and X.L.Wang, 1995: Sensitivity of systematic error of extended range forecasts to sea surface temperature anomalies. *J.Climate*, **8**, 1533-1543.

Molteni, F., S.Tibaldi and T.N.Palmer, 1990: Regimes in the wintertime circulation over northern extratropics. I: Observational evidence. *Q.J.R.Meteorol.Soc.*, **116**, 31-67.

Molteni, F., R.Buizza, T.N.Palmer and T.Petroliagis, 1994: The ECMWF ensemble prediction system: methodology and validation. *Q.J.R.Meteorol.Soc.* (to appear).

Morcrette, J.-J., 1993: Revision of the clear-sky and cloud radiative properties in the ECMWF model. *ECMWF Newsletter*, **61**, 3-14.

Palmer, T.N., Č.Branković, F.Molteni and S.Tibaldi, 1990: Extended-range predictions with ECMWF models: Interannual variability in operational model integrations. *Q.J.R.Meteorol.Soc.*, **116**, 799-834.

Tibaldi, S. and F.Molteni, 1990: On the operational predictability of blocking. *Tellus*, **42A**, 343-365.

Viterbo, P. and A.C.M.Beljaars, 1995: An improved land surface parametrization scheme in the ECMWF model and its validation. *J.Climate*, **8**, (in press).

Table 1 Principal changes to the model formulation from cycle 36 to cycle 12r1.

Model cycle	Date	Modifications
36	5 Jun 1990	- Surface fluxes for low wind speed over sea - Convective cloud formulation - Implicit gravity wave drag introduced
37	12 Feb 1991	- Technical changes
38	9 Apr 1991	- Maximum overlap of cloud layers - Cooling to space above 10 mb - Vertical diffusion above PBL - Revised convection
39	17 Sep 1991	- Semi-Lagrangian scheme, reduced grid, T213 model, 31 levels - New horizontal diffusion (T213 only) - Cloud scheme modified - Timestep-dependent convective mass flux limit - Partially implicit normal mode initialisation
40	26 Nov 1991	- Corrected bug in long-wave radiation
41	7 Jan 1992	- Horizontal diffusion modified (T213 only) - Time-stepping algorithm for cumulus momentum transfer changed
42	13 May 1992	- Mass flux limit in convective parametrization corrected - Treat sea ice as land in free convective regime - Virtual temperature as spectral variable - Optimised semi-Lagarangian trajectory calculations, optimised radiation
43	17 Aug 1992	- Vertically non-interpolating semi-Lagrangian scheme, smaller time filter - Explicit time scheme for cumulus momentum transfer - Changes to sea ice parametrization - Modified treatment of low-level inversion clouds - Consistent interpolation between full and half level temperatures in radiation
44	1 Sep 1992	- Technical changes
45	7 Dec 1992	- Technical changes
46	1 Feb 1993	- Include short wave optical properties for ice and mixed phase clouds - Revise clear sky absorption - Pure del 4 horizontal diffusion (T213 only)
47	21 Apr 1993	- Technical changes
48	4 Aug 1993	- Entrainment at top of PBL - Increased entrainment in shallow convection - Modified roughness length and air-sea transfer coefficients - New parametrization of soil processes
49	5 Oct 1993	- Changes to skin and 2 m temperature profile function
11r7	2 Mar 1994	- New closure in shallow convection - Inclusion of latent heat release due to freezing of condensate in convective updrafts - Distinction between water and ice clouds in radiation scheme changed
12r1	23 Aug 1994	- Technical changes

Table 2 The 500 mb height correlation coefficients between observed anomalies and model ensemble mean errors for El Niño and La Niña winters.

	DJF 1986/87		DJF 1988/89	
	PNA	Atlantic/Europe	PNA	Atlantic/Europe
CY36	-0.45	-0.67	0.02	-0.48
CY48	-0.68	-0.80	-0.60	-0.56
12r1	-0.15	-0.66	-0.18	-0.35

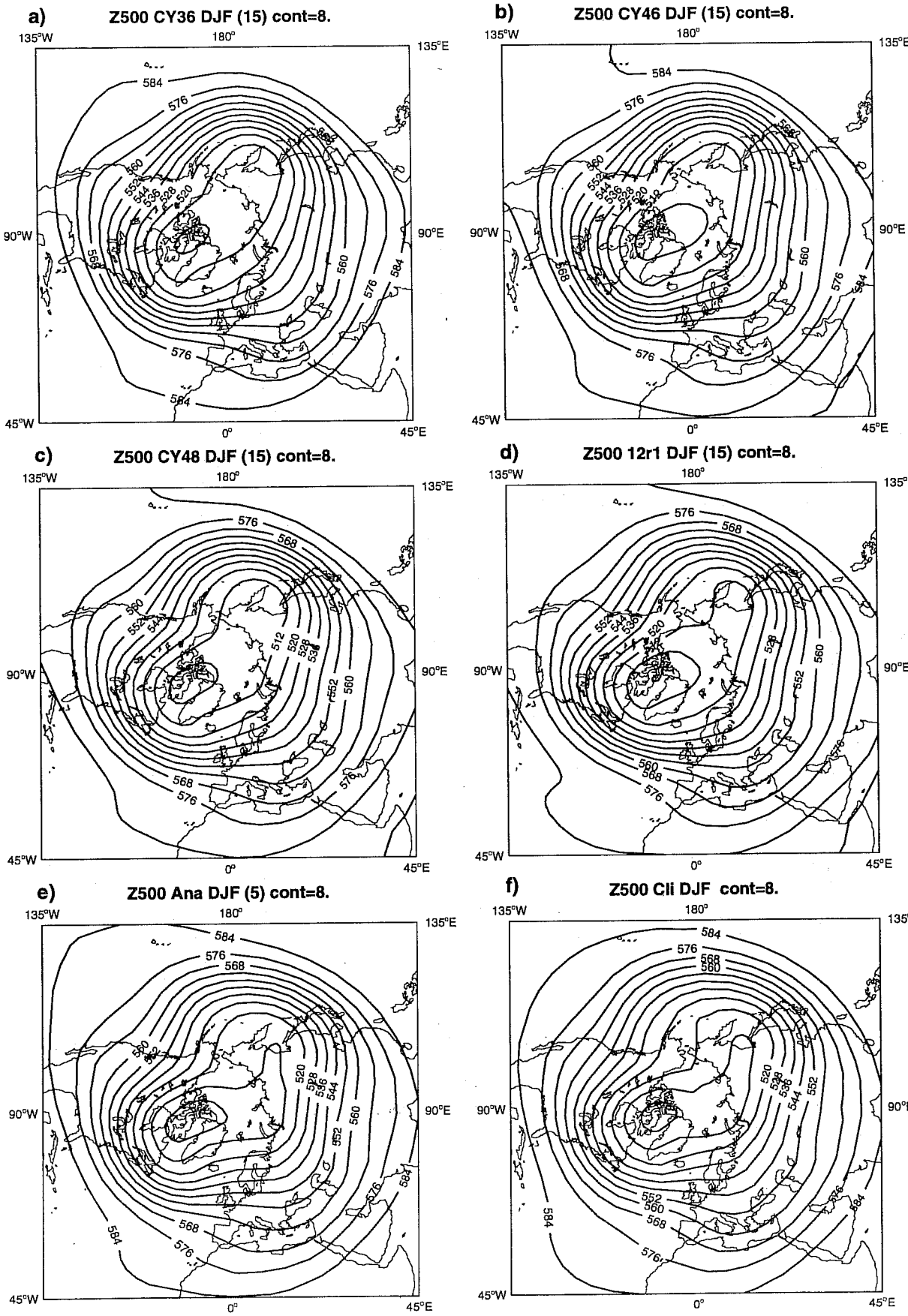

Fig.1 Ensemble mean DJF 500 mb height fields for model cycle: a) CY36, b) CY46, c) CY48, d) 12r1, e) ECMWF 5-year mean analysis and f) ECMWF 12-year mean analysis. Contours every 8 dam.

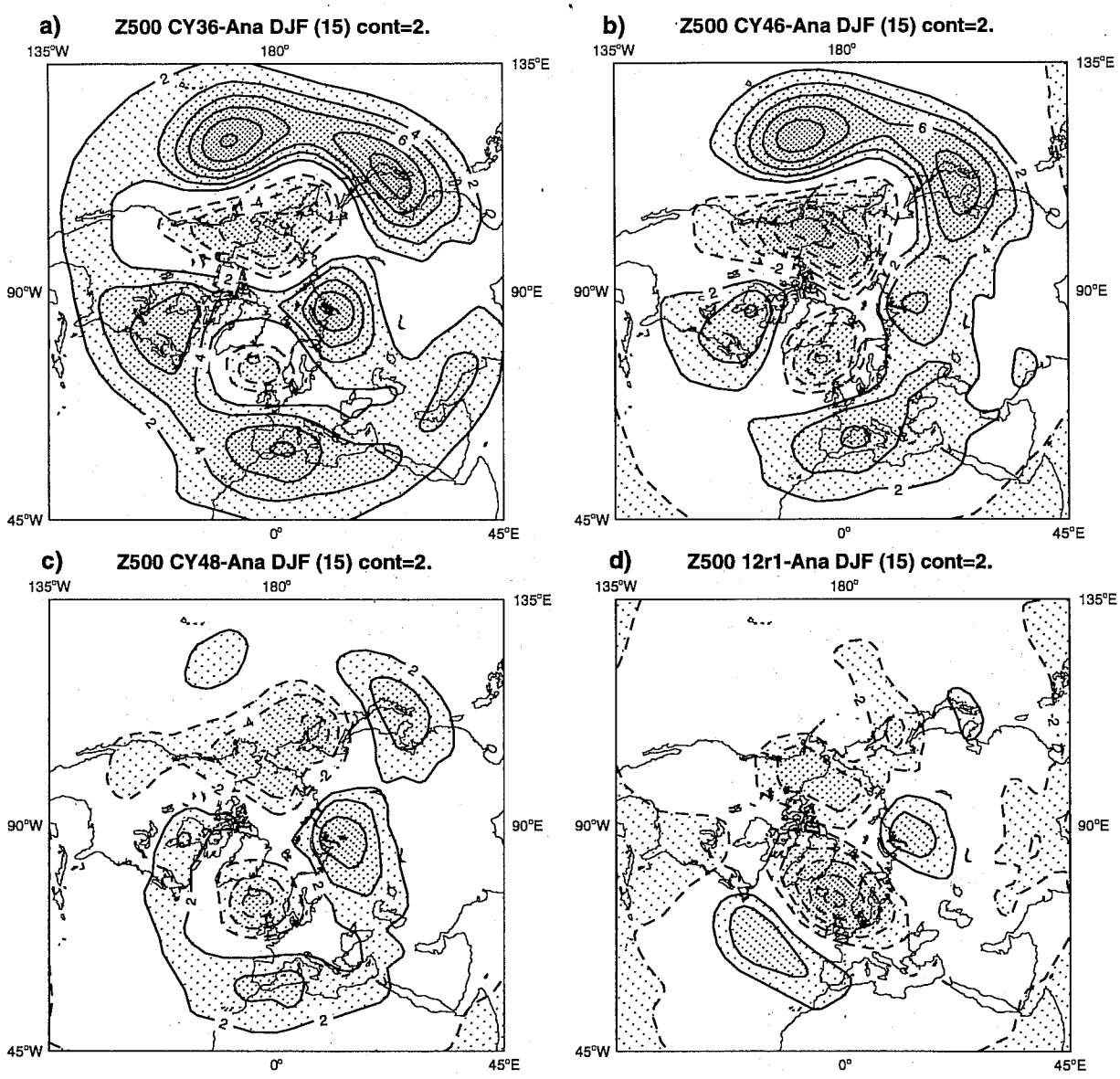

Fig.2 Ensemble mean error fields of DJF 500 mb height for model cycle: a) CY36, b) CY46, c) CY48, d) 12r1. e) to h) as a) to d) but for the southern hemisphere. Solid positive errors, dashed negative errors. Contours every 2 dam.

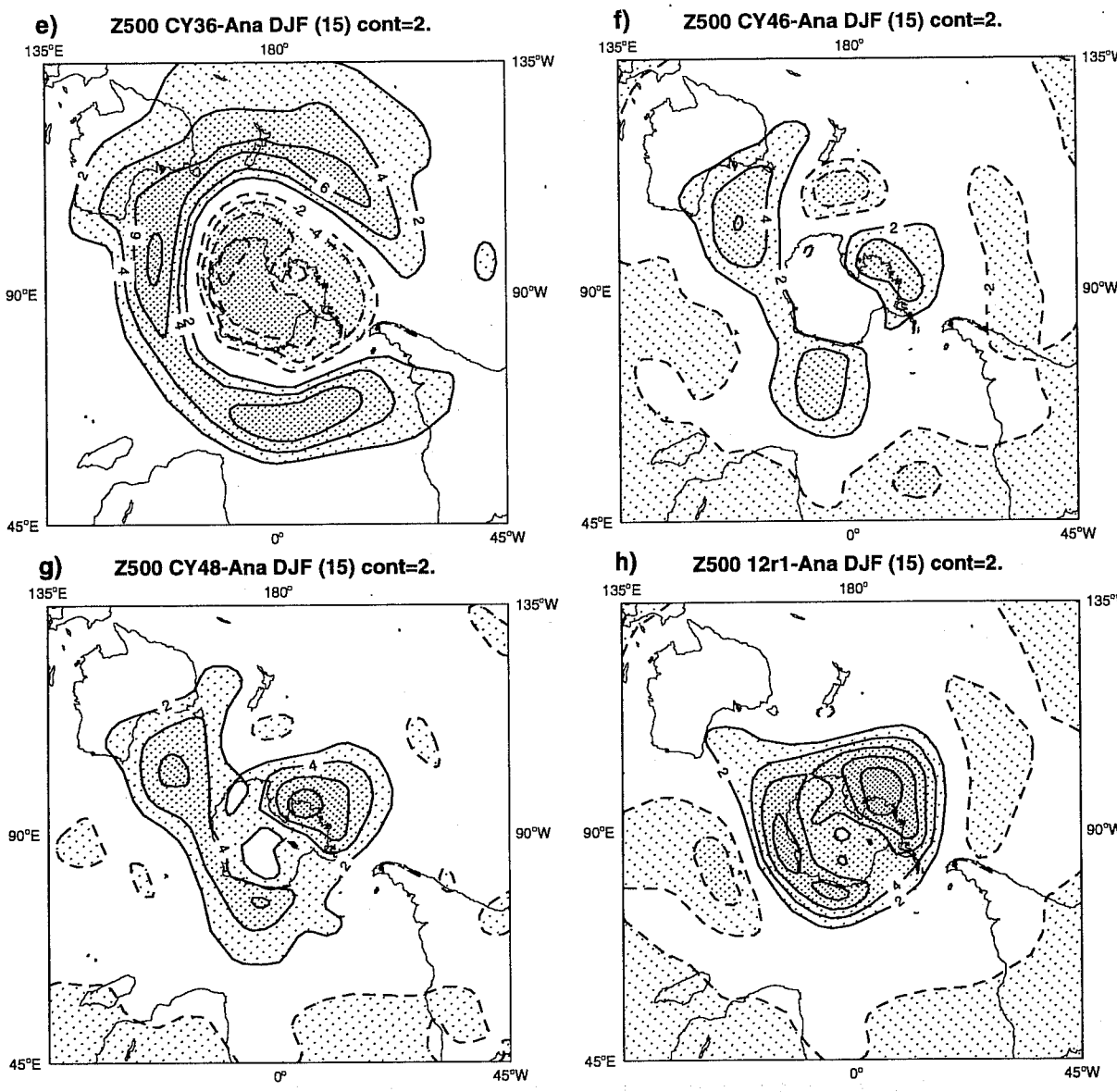

Fig.2 continued.

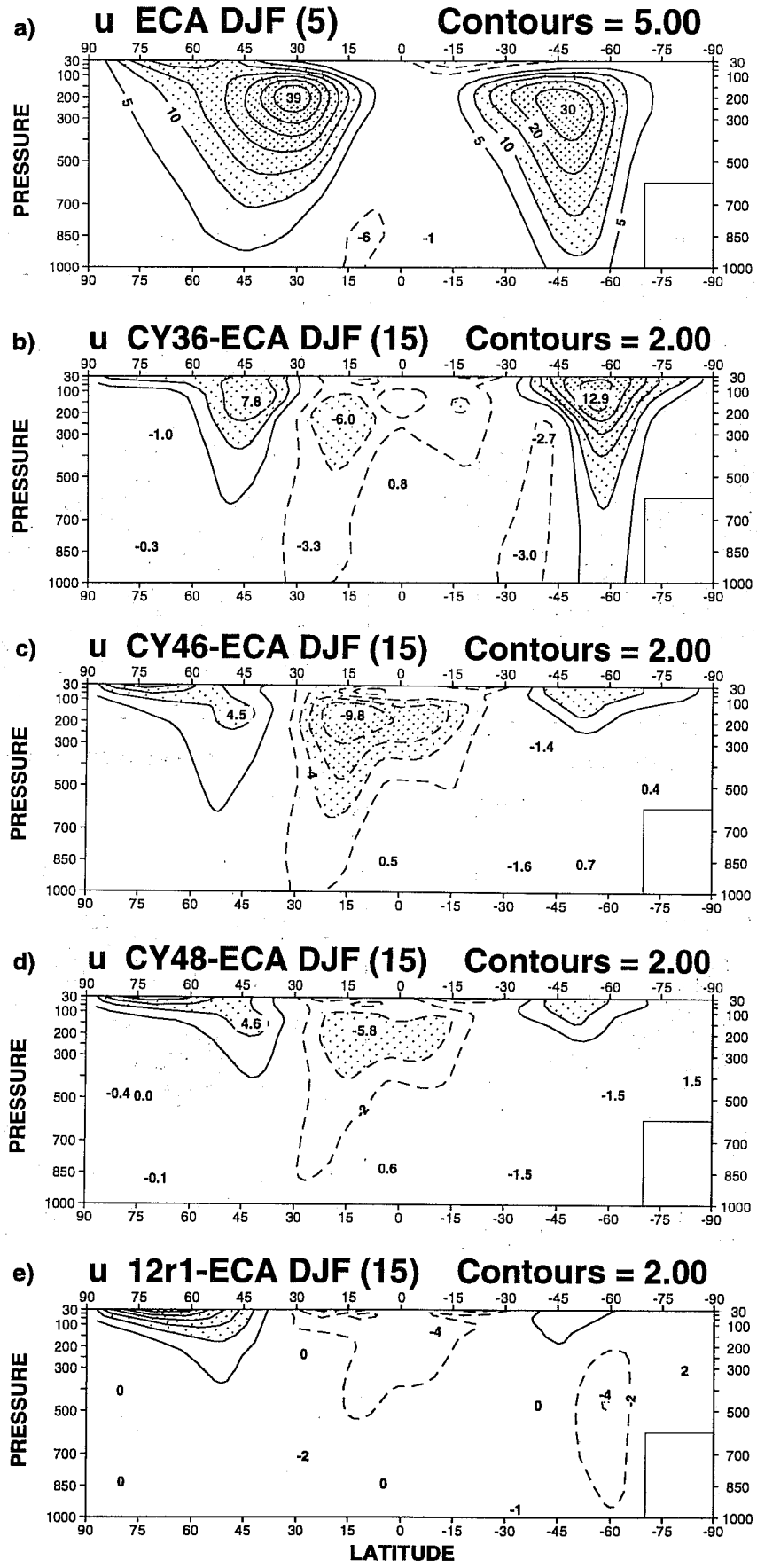

Fig.3 Zonally averaged cross sections of ensemble mean DJF zonal wind for: a) ECMWF 5-year mean. Errors for model cycle: b) CY36, c) CY46, d) CY48 and e) 12r1. Solid westerlies and positive errors, dashed easterlies and negative errors. Contours every 5 ms^{-1} in a) and every 2 ms^{-1} in b) to e).

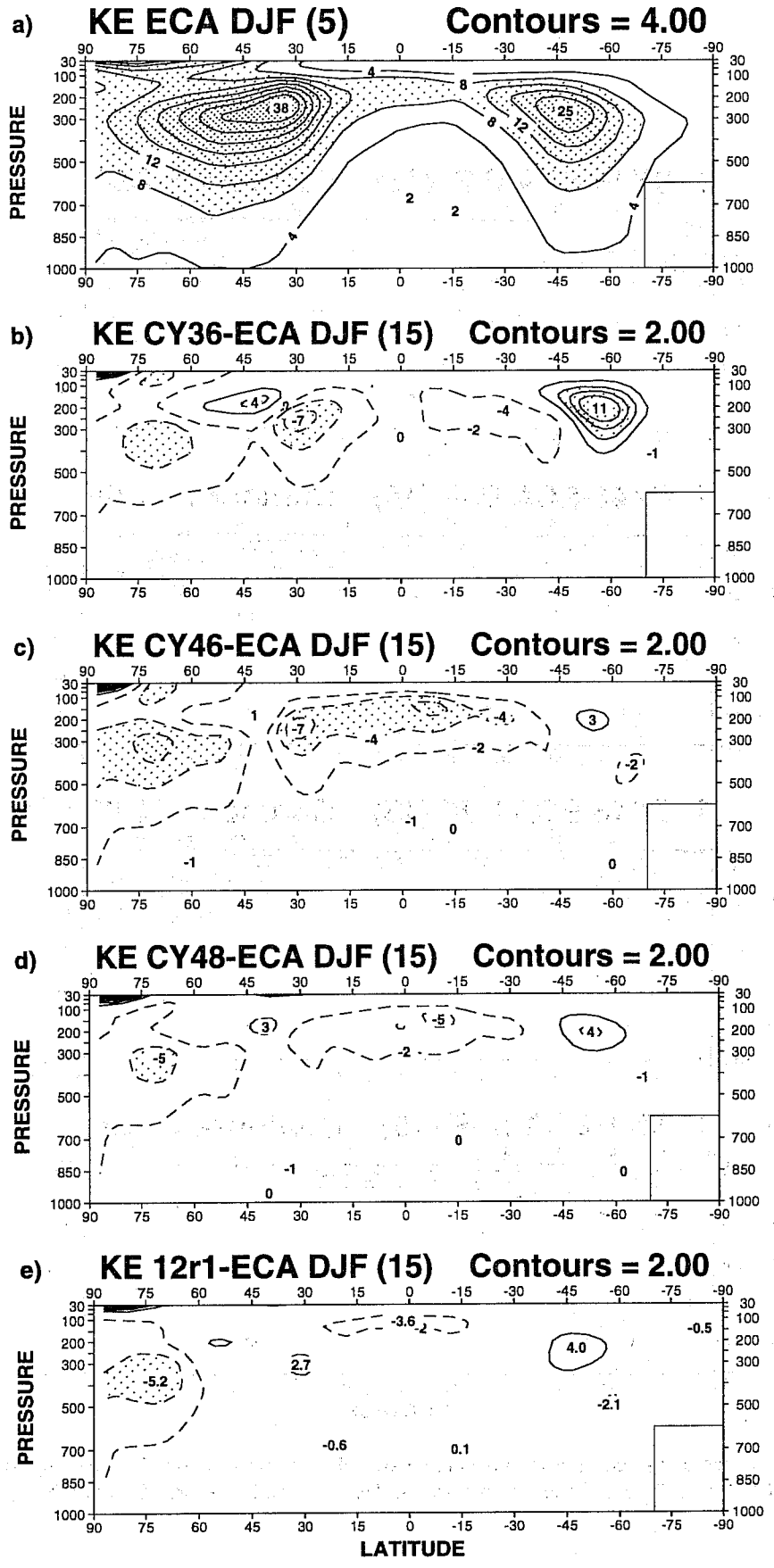

Fig.4 As Fig.3 but for eddy kinetic energy. Solid positive errors, dashed negative errors. Contours every 4 $Jm^{-2}Pa^{-1}$ in a) and every 2 $Jm^{-2}Pa^{-1}$ in b) to e).

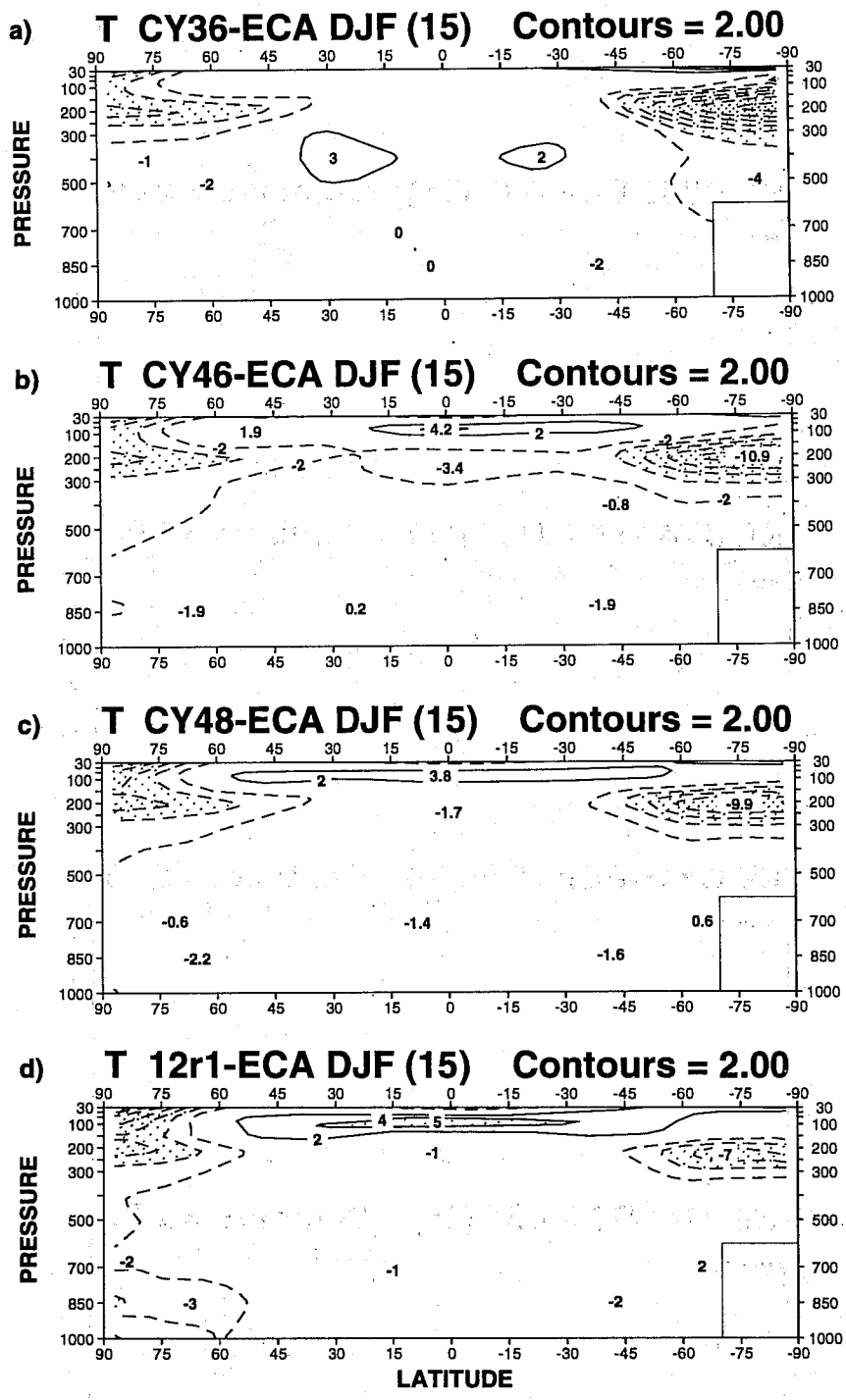

Fig.5 Zonally averaged cross sections of ensemble mean DJF temperature error for model cycle: a) CY36, b) CY46, c) CY48 and d) 12r1. Solid positive errors, dashed negative errors. Contours every 2 K.

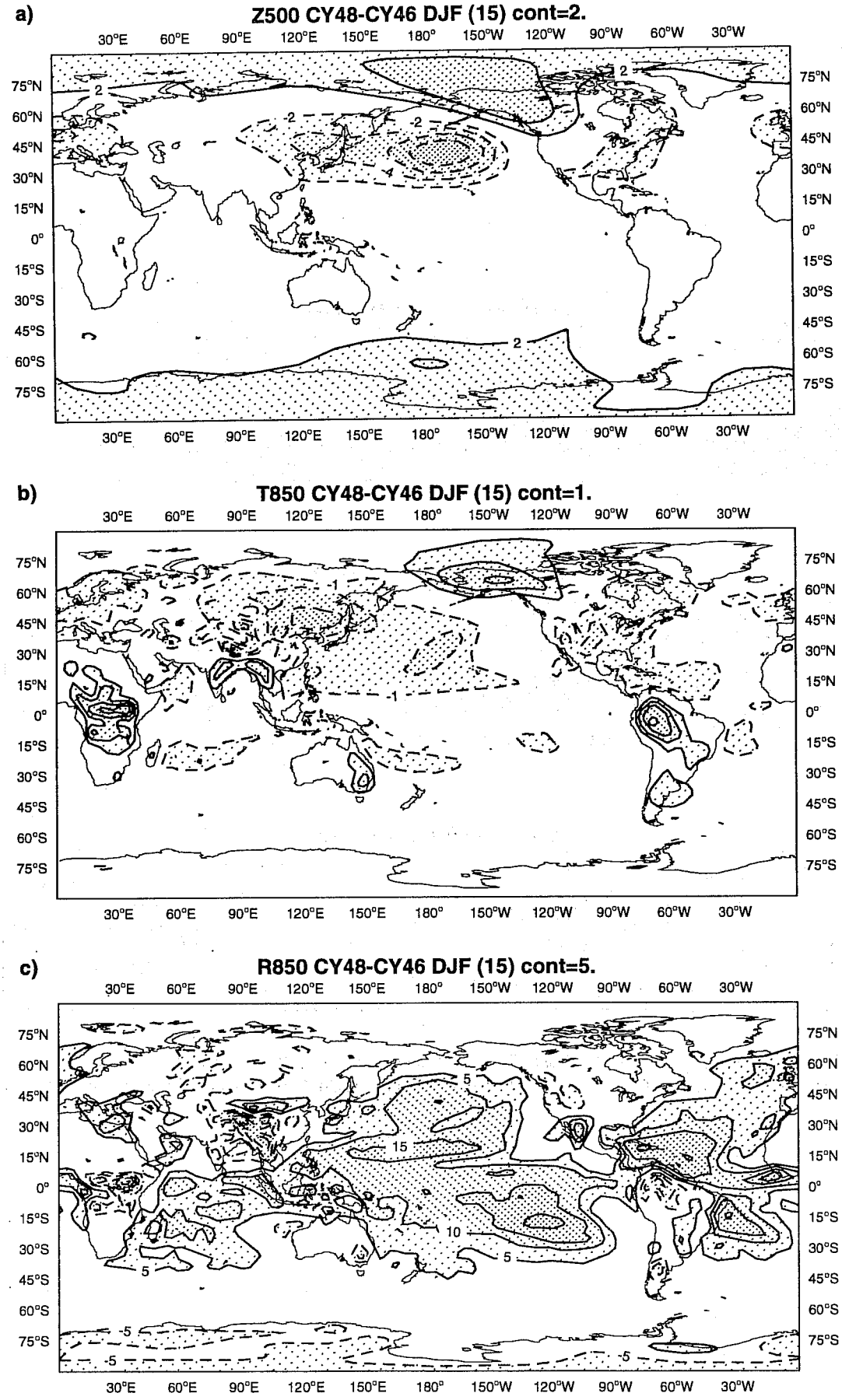

Fig.6 Ensemble mean DJF difference fields for CY48 minus CY46: a) 500 mb height, b) 850 mb temperature and c) 850 mb relative humidity. Solid positive differences, dashed negative differences. Contours every 2 dam in a), 1 K in b) and 5% in c).

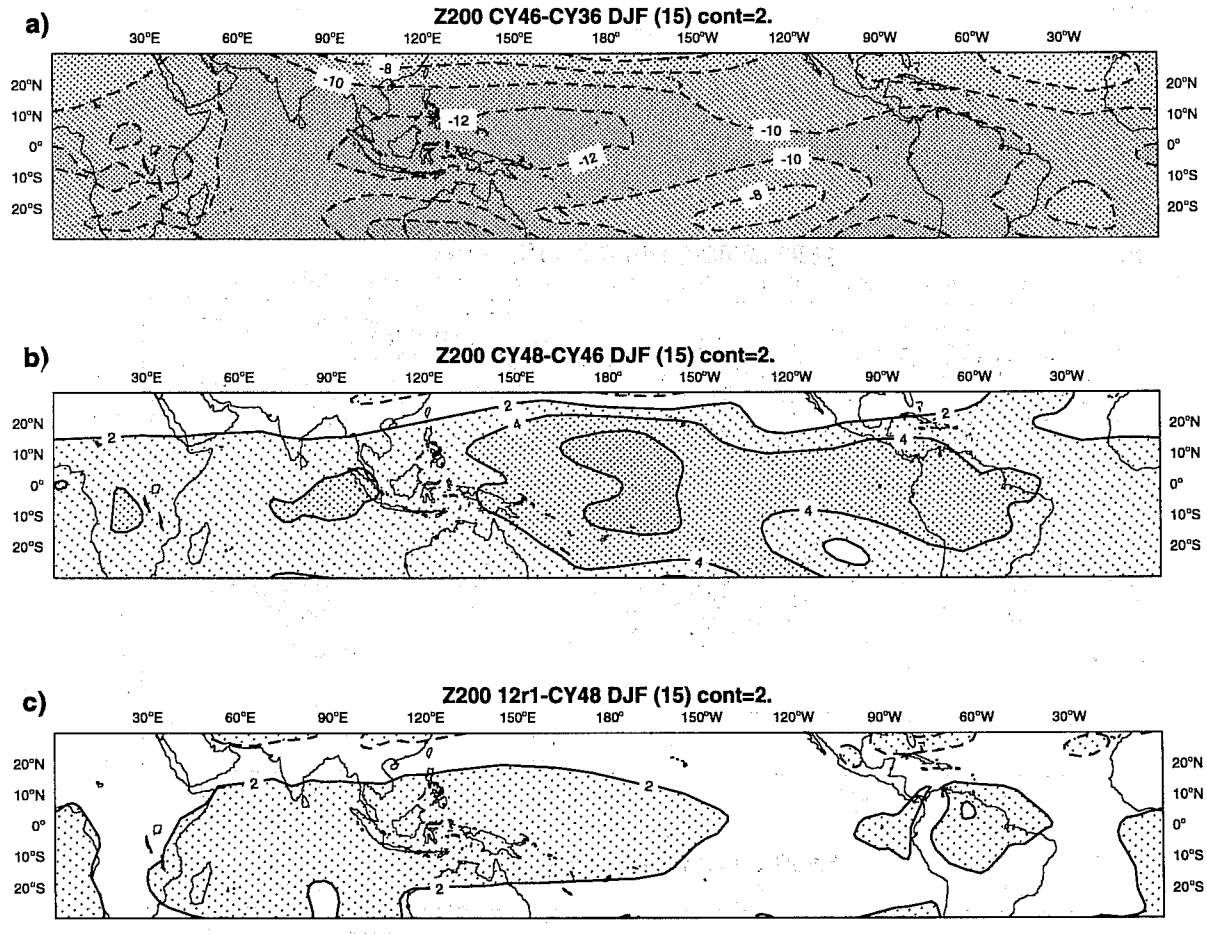

Fig.7 Ensemble mean DJF 200 mb height difference fields for a) CY46 minus CY36, b) CY48 minus CY46 and c) 12r1 minus CY48. Solid positive differences, dashed negative differences. Contours every 2 dam.

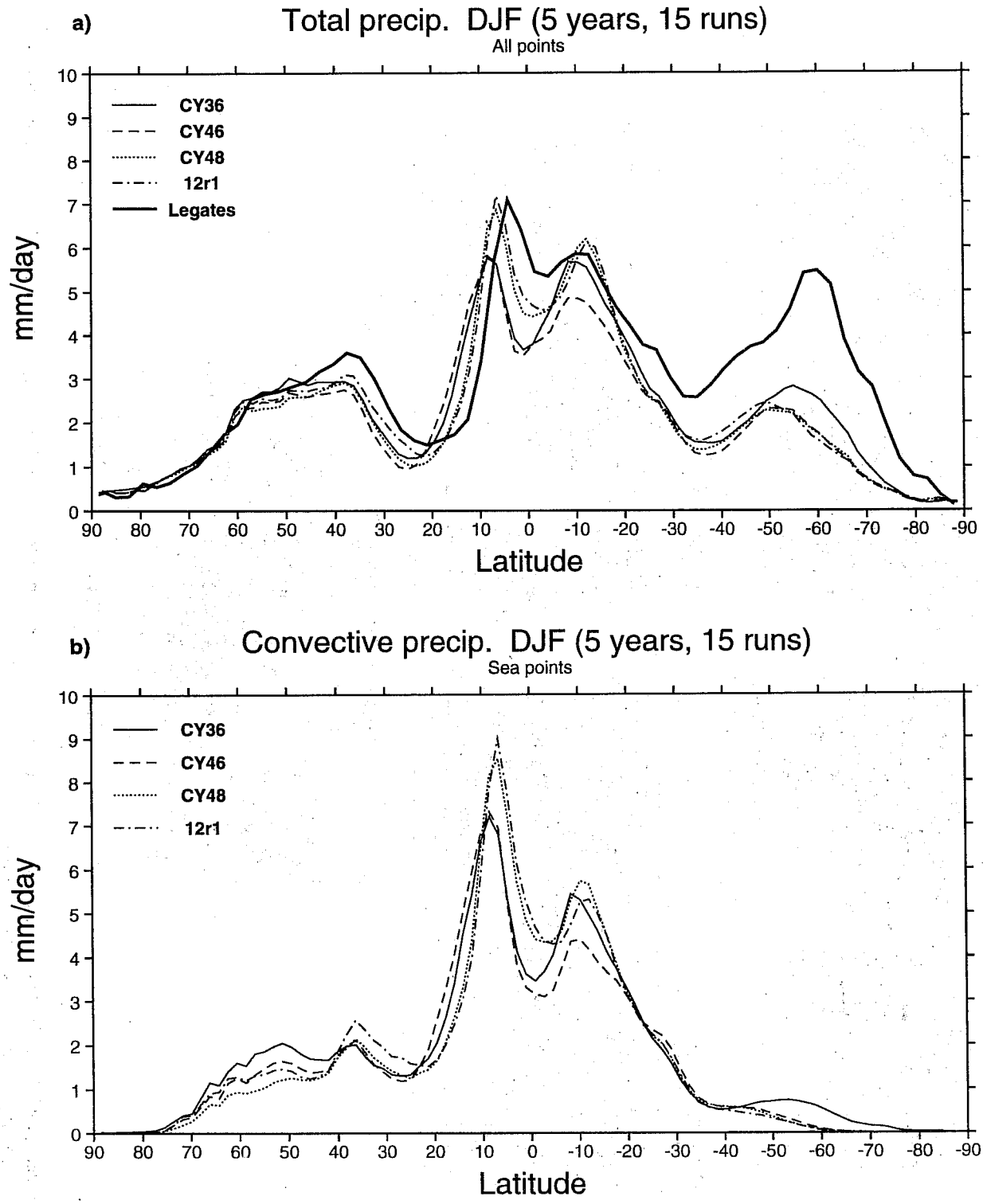

Fig.8 Zonally averaged ensemble mean DJF precipitation: a) total over all points, b) convective over sea points only. Units mmday^{-1}.

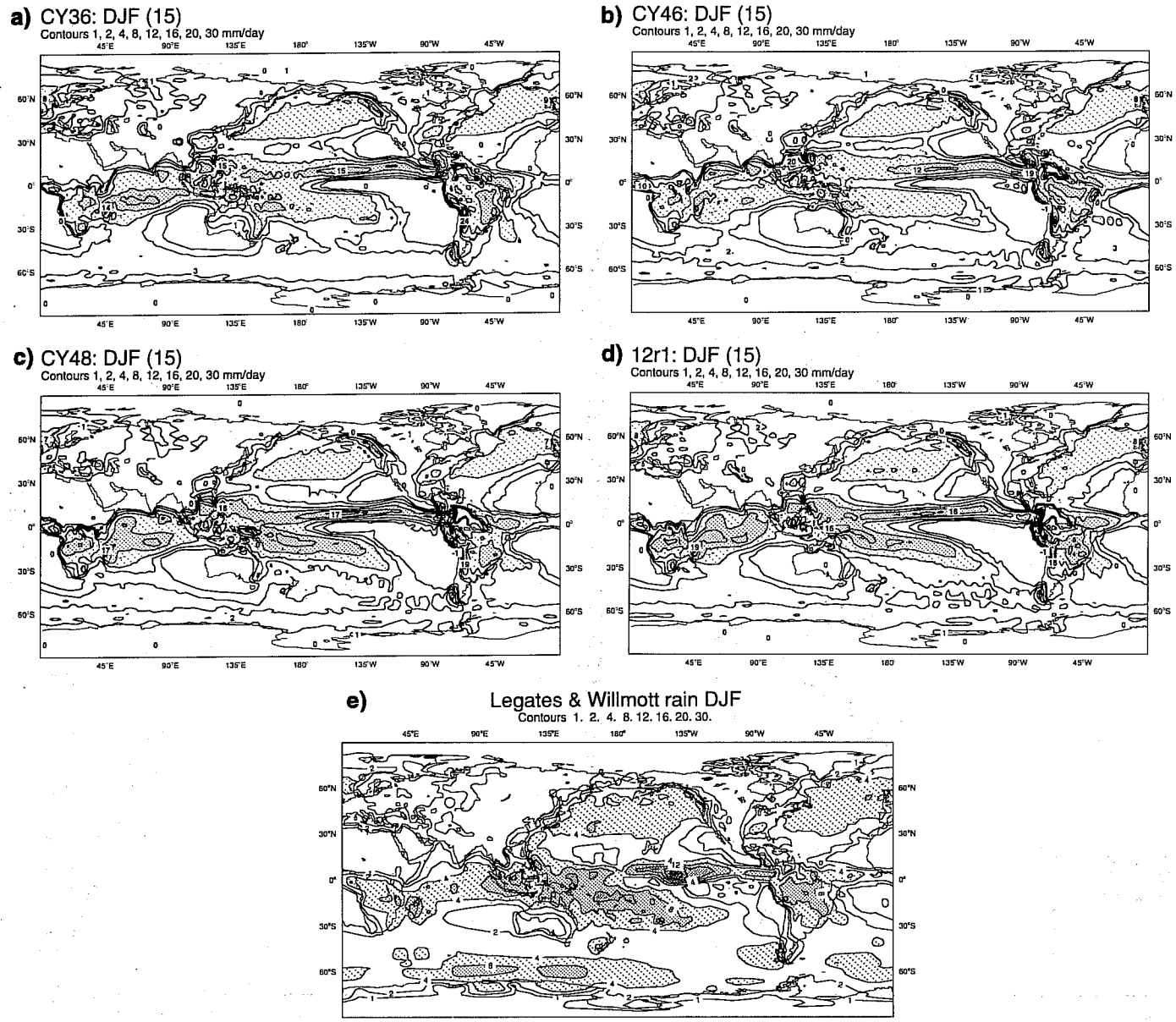

Fig.9 Ensemble mean DJF total precipitation fields for model cycle: a) CY36, b) CY46, c) CY48, d) 12r1 and e) climatology (Legates and Willmott 1990). Contours: 1, 2, 4, 8, 12, 20 and 30 mmday^{-1}. Amounts larger or equal to 4 mmday^{-1} are shaded.

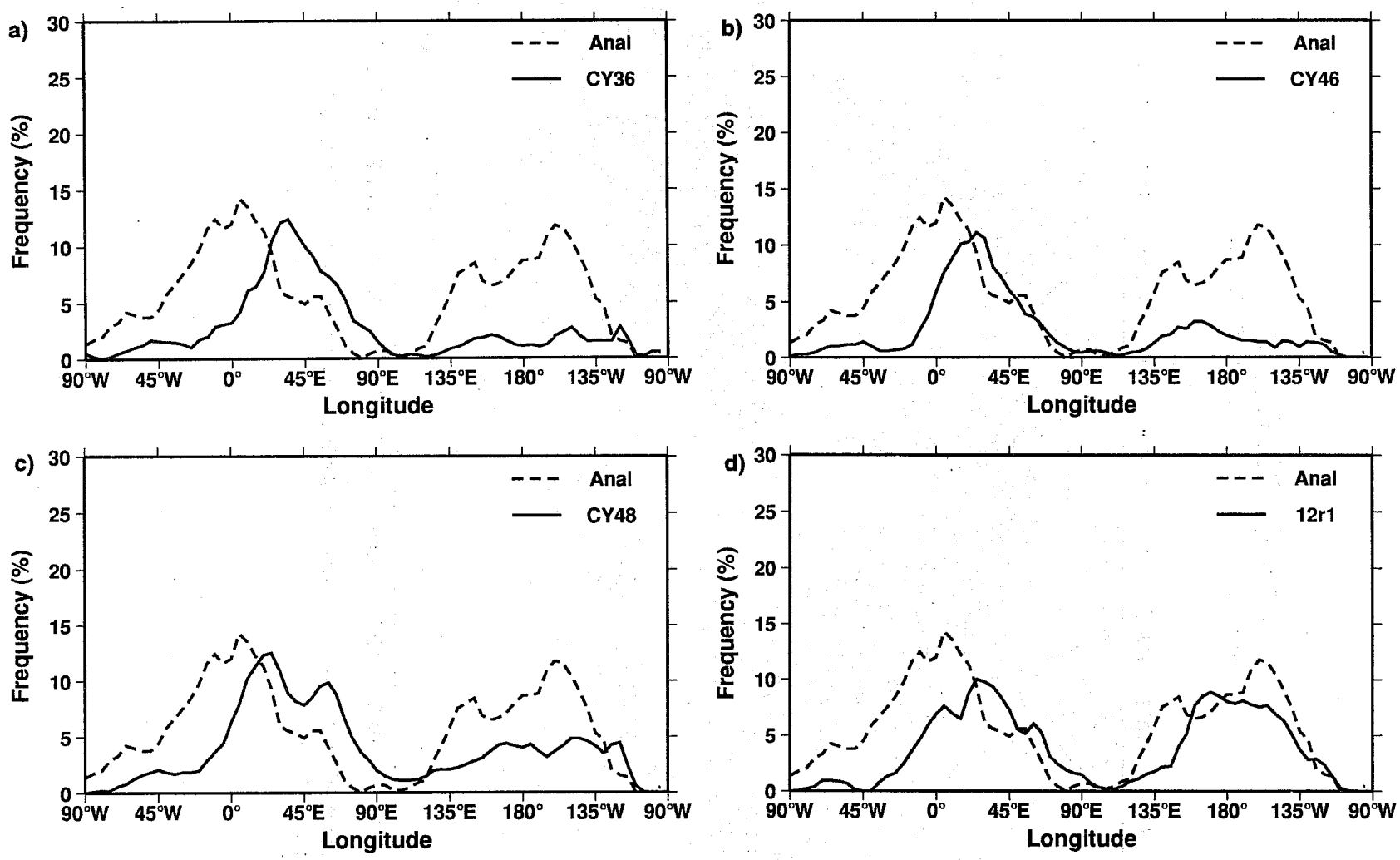

Fig.10 Frequency (in %) of occurrence of blocking as defined by Tibaldi and Molteni (1990) for DJF ensembles of model cycle: a) CY36, b) CY46, c) CY48 and d) 12r1. Dashed 5-year analysis mean.

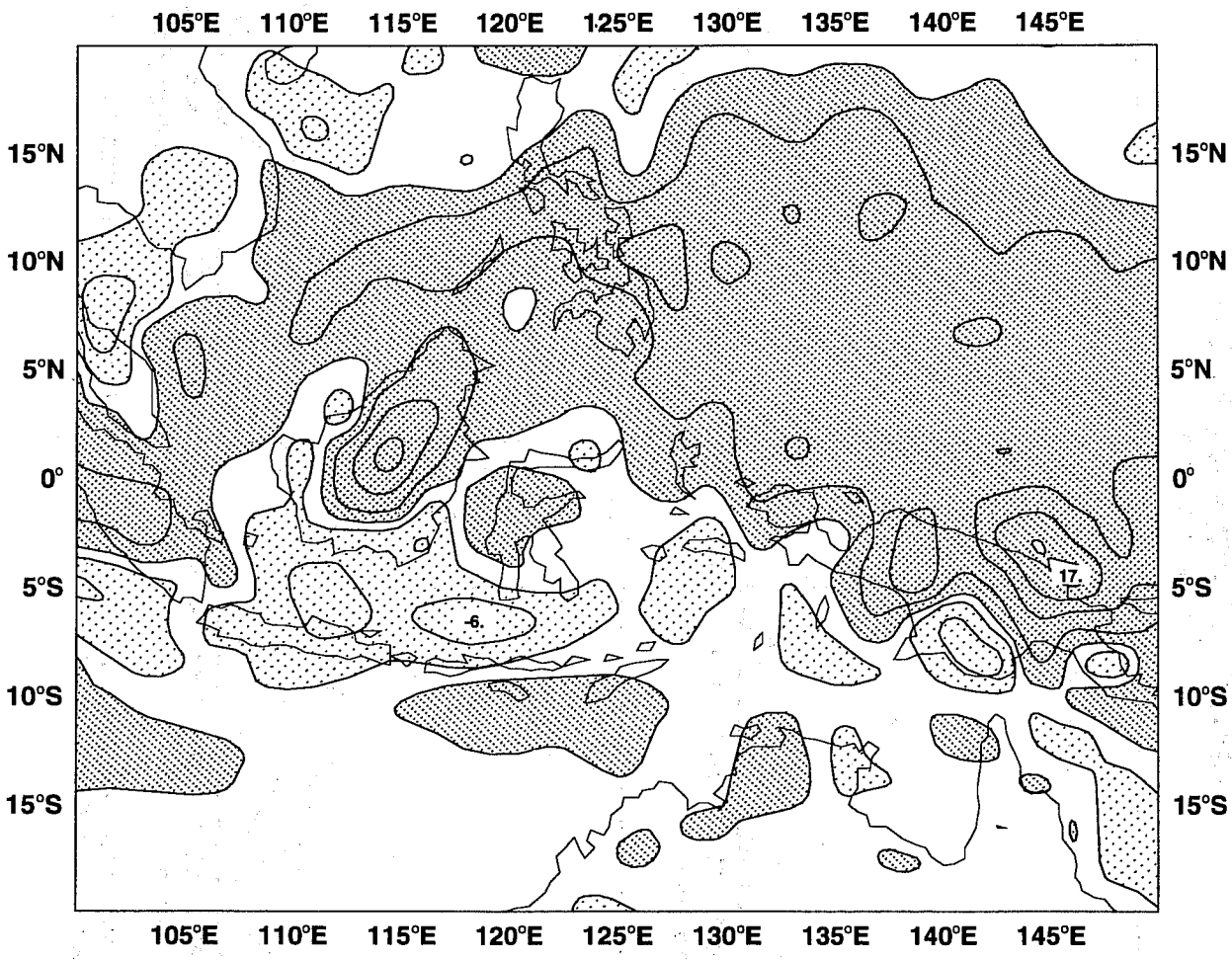

Fig.11 Ensemble mean DJF precipitation difference fields for cycle 12r1 minus CY36. Contours ±1, ±4, ±8, ±12 and ±16 mmday^{-1}.

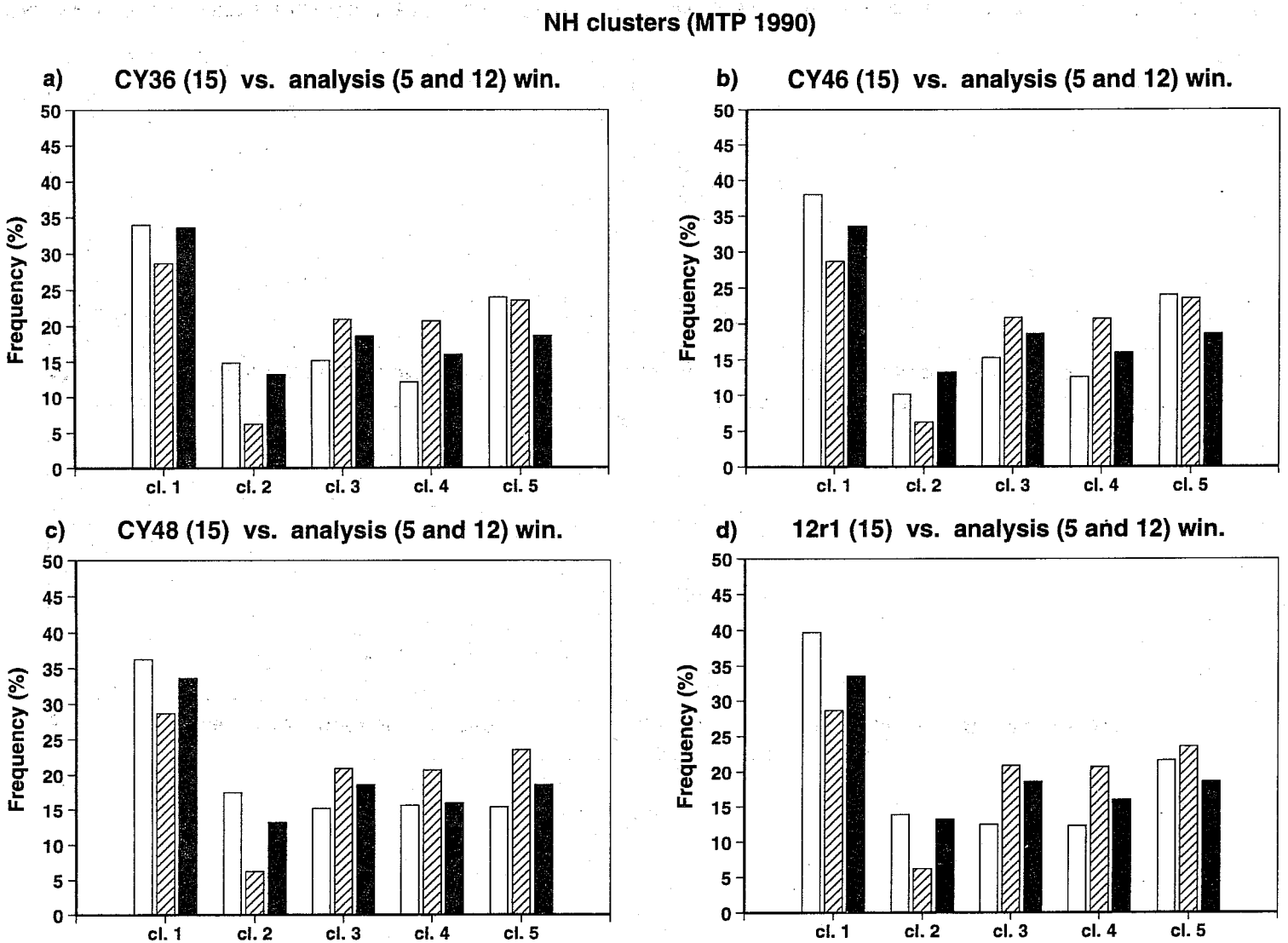

Fig.12 Frequency (in %) of planetary clusters as defined by Molteni *et al.* (1990) for DJF ensembles of model cycle (left-hand bars): a) CY36, b) CY46, c) CY48 and d) 12r1. Centre bars analysis from 5-year average, right-hand bars analysis from 12-year average.

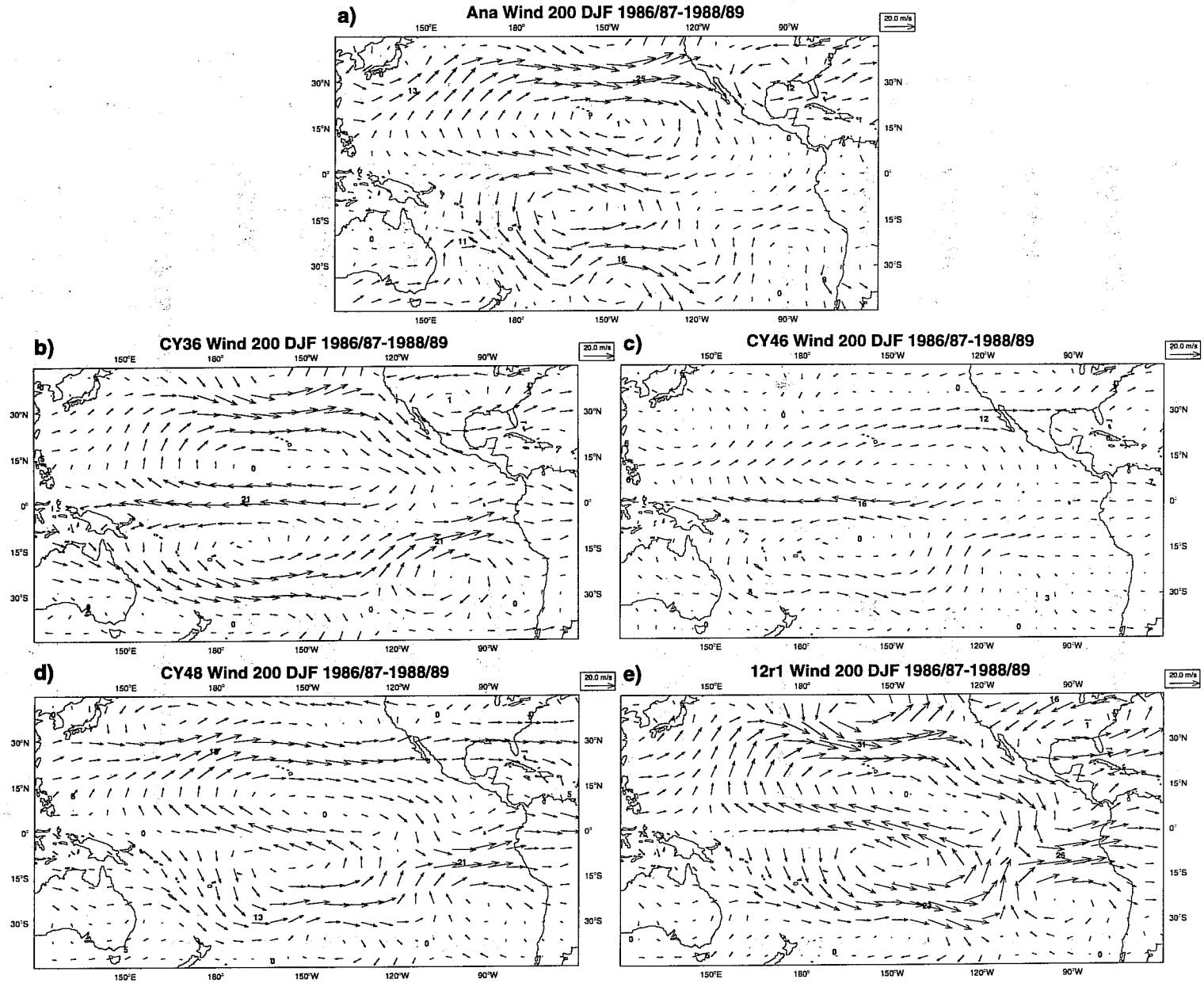

Fig.13 200 mb wind difference fields DJF 1986/87 minus DJF 1988/89 for a) ECMWF analysis and for 3-member ensemble mean model cycle: b) CY36, c) CY46, d) CY48 and e) 12r1.

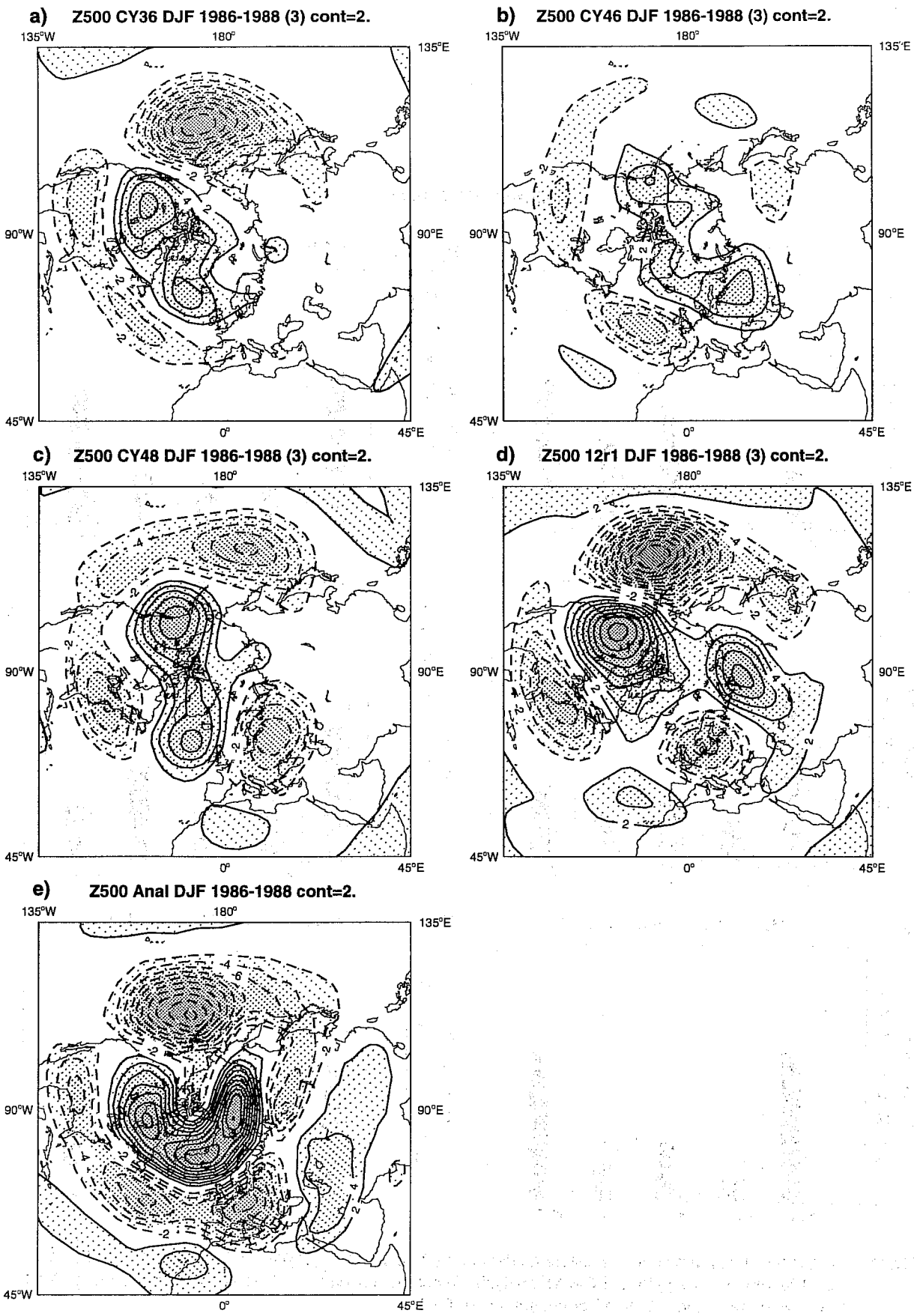

Fig.14 3-member ensemble mean 500 mb height difference fields DJF 1986/87 minus DJF 1988/89 for model cycle: a) CY36, b) CY46, c) CY48, d) 12r1 and for e) ECMWF analysis. Solid positive differences, dashed negative differences. Contours every 2 dam.

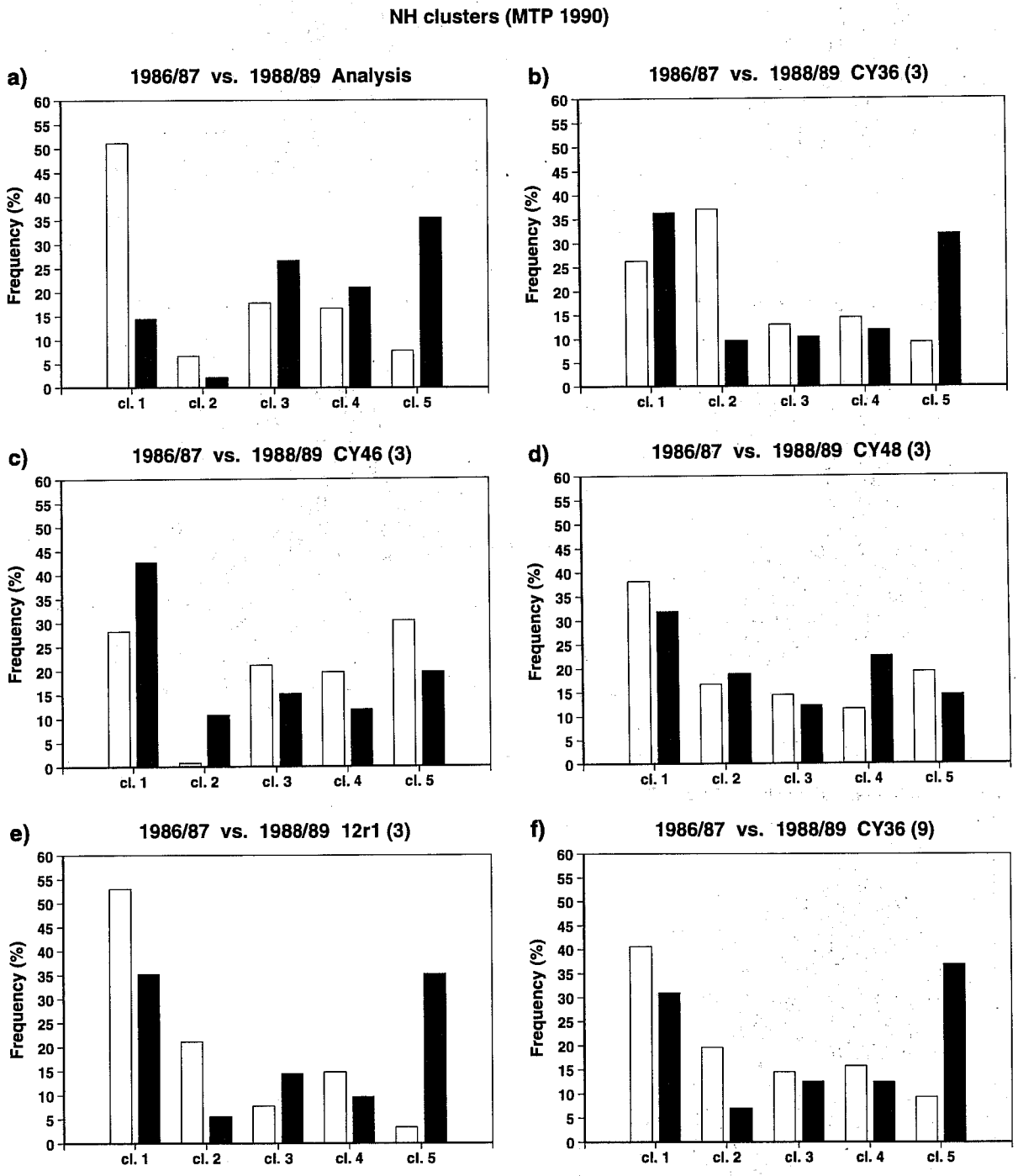

Fig.15 Frequency (in %) of planetary clusters as defined by Molteni *et al.* (1990) for DJF 1986/87 (left bars) vs. DJF 1988/89 (right bars) for a) ECMWF analysis; 3-member ensembles of model cycle: b) CY36, c) CY46, d) CY48, e) 12r1 and f) 9-member ensembles of CY36.

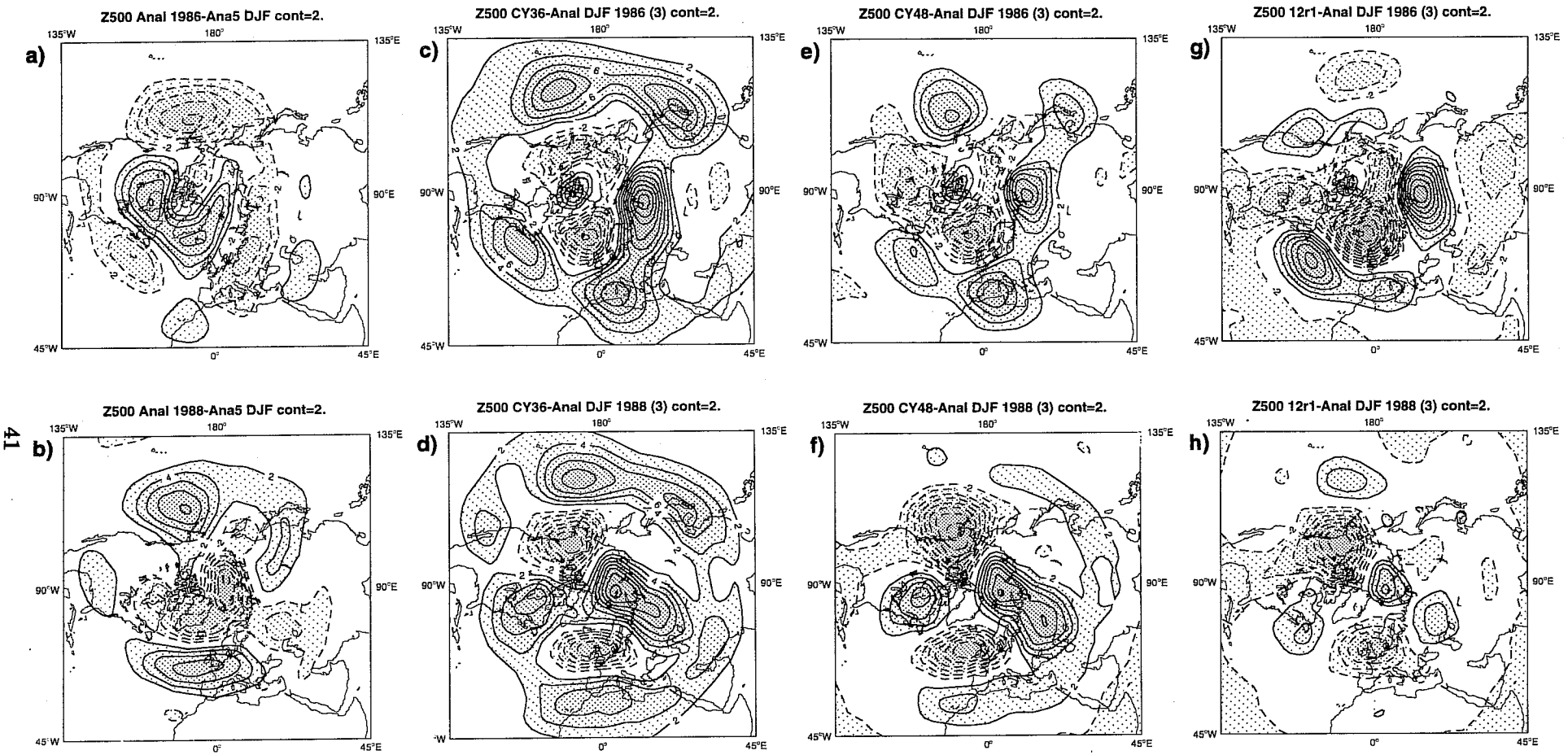

Fig.16 DJF 500 mb height observed anomaly for a) 1986/87, b) 1988/89; 3-member ensemble mean DJF 500 mb height error for c) CY36 1986/87, d) CY36 1988/89, e) CY48 1986/87, f) CY48 1988/89, g) 12r1 1986/87 and h) 12r1 1988/89. Solid positive anomalies/errors, dashed negative anomalies/errors. Contours every 2 dam.